X-721-66-395

NASA TM X-55562

THE EFFECT OF ANTENNA LOCATION ON PITCH/ROLL COUPLING CHARACTERISTICS ON THE APACHE

AUGUST 1966

NASA — GODDARD SPACE FLIGHT CENTER

GREENBELT, MARYLAND

X-721-66-395

THE EFFECT OF ANTENNA LOCATION ON PITCH/ROLL COUPLING CHARACTERISTICS OF THE APACHE

Edward E. Mayo and Mark B. Nolan

Sounding Rocket Branch
Spacecraft Integration and Sounding Rocket Division

August 1966

GODDARD SPACE FLIGHT CENTER
Greenbelt, Maryland

THE EFFECT OF ANTENNA LOCATION ON PITCH/ROLL COUPLING CHARACTERISTICS OF THE APACHE

Edward E. Mayo and Mark B. Nolan

Sounding Rocket Branch
Spacecraft Integration and Sounding Rocket Division

ABSTRACT

Data from wind-tunnel testing have been used in equilibrium solutions and dynamic simulations to assess the effects of forward-mounted quadraloop antennas on the pitch/roll coupling characteristics of the Apache.

CONTENTS

ILLUSTRATIONS

ILLUSTRATIONS (Cont'd)

SYMBOLS

Alt.	Altitude (feet)
C_A	Axial force coefficient
ΔCG	Lateral center-of-gravity offset (inches)
C_{L_α}	Lift curve slope, per radian
C_l	Roll-forcing coefficient
C_{l_i}	Induced rolling moment coefficient
C_{l_p}	Roll-damping coefficient, $C_{l_p} = \partial C_l / \partial \left(\frac{pd}{2V}\right)$
C_{m_α}	Static stability parameter, per radian
C_{m_q}	Pitch-damping derivative, $C_{m_q} = \partial C_m / \partial \left(\frac{qd}{V}\right)$
DIM A	Tab height setting (inches)
d	Base diameter (feet)
I	Pitch inertia (slugs/ft^2)
I_{xx}	Roll inertia (slugs/ft^2)
LUPWT	Langley unitary plan wind tunnel
M	Mach number
p	Roll rate
p_u	Undisturbed roll rate (not influenced by C_{l_i}, ΔCG, or thrust misalignment)
q	Pitch rate (rad/sec)
q_∞	Dynamic pressure (lb/ft^2)
t	Time (seconds)

SYMBOLS (Cont'd)

V	Velocity (feet per second)
α_{ST}	Non-rolling trim (degrees)
α_T	Rolling trim (degrees)
ω	Undamped pitch frequency
ϕ	Rolling trim orientation (degrees)
ϕ_o	Non-rolling trim orientation (degrees)

THE EFFECT OF ANTENNA LOCATION ON PITCH/ROLL COUPLING CHARACTERISTICS OF THE APACHE

INTRODUCTION

The Nike Apache is the vehicle most widely used in the sounding-rocket program. The most persistent and unsolved problem concerning its performance is its roll-rate history and, consequently, its pitch/roll coupling characteristics.

Several reports have attempted unsuccessfully to explain the roll-rate abnormality (1, 2, 3). Flight experience and the use of analytical means have made it possible to predict the roll rate at strategic points during the trajectory — Nike burnout, Apache ignition, and post-burnout — and have led to recommended roll requirements and spin tab-setting charts (3, 4). Although these recommended roll procedures have resulted in a highly successful flight record, several flight failures have occurred, most of which have been attributed to forward-mounted quadraloop antennas. Since in-house calculations indicated that the increased loading and loss in stability caused by these small "canards" was not sufficient to cause flight failure, a wind-tunnel test (5) was conducted to determine if these devices could produce induced roll moments sufficiently large to cause roll lock-in and catastrophic yaw.

The test results showed that the maximum induced roll moment near resonance for the quadraloop-forward location was approximately twenty times the clean-configuration value, and that the induced roll-moment coefficient period was determined by the quadraloops rather than by the number of fins (i.e., π instead of $\pi/2$). The tests showed no degradation in induced roll moment when the quadraloops were located in the rearward position. The tests also provided information on the increased loading and loss in stability caused by the antennas. For the quadraloop configurations tested, the antenna loading was a maximum of 60 percent of the lift provided by the clean body alone, and the loss in stability was about 1 caliber.

The analysis described in this report was to determine the effects of antenna location on pitch/roll coupling characteristics of the Apache, and to establish the allowable lateral center-of-gravity offset for breaking out of roll lock-in.

ANALYSIS

The analyses presented here parallel the approach taken in (6) and (7). The small-angle approximation computer program of (8), modified as described in (7)

and adapted to our computer according to (9) and (10), was used in computing the angular motions about the prescribed trajectory.

Conditions of Study

Study Model and Trajectory — Figure 1 shows the model chosen for study, a nominal 80-pound 60-inch-long payload. This configuration was chosen because most of the required input data* were retrievable from a previous 6-degree-of-freedom run. The atmospheric environment (velocity and altitude history) was extracted from an 80-degree sea-level-launch particle trajectory.

Misalignments — A 0.116-degree angular thrust misalignment and 0.02-inch thrust eccentricity was assumed with the point of application at the base of the vehicle. An average thrust of 4775 pounds was applied over the burn-time interval of from 20 to 26.4 seconds. This corresponds to a total impulse of 30,577 lb. sec. An aerodynamic misalignment moment coefficient, C_{m_o}, of 0.5 was assumed. This corresponds to a fin misalignment of 0.1 degree at Apache ignition, or a non-rolling static trim of 0.23 degree at booster separation, 0.14 degree at Apache ignition, 0.54 degree at Apache burnout, and 0.39 degree at $t = 40$ seconds. The thrust and aerodynamic misalignments were deduced from those used in dispersion studies by Sandia Corporation (11). The study reported here always assumed the misalignments to be in the worst possible orientation. A nominal center-of-gravity location 6.2 feet ahead of the base was assumed.

Undisturbed Roll Rates — Figure 2 shows a comparison of the undisturbed roll rate and undamped pitch rate. The roll rates were determined from dynamic simulations assuming zero induced roll moments, zero center-of-gravity offset, and no thrust misalignment. Although these roll rates are not typical of most flights (3), it will be shown later that the success or failure of a flight depends upon the peak roll rate at Apache ignition, and the minimum frequency increment between the undisturbed roll and undamped pitch frequencies during second-stage burn. Hence, the exact shape of the curve is immaterial.

Equilibrium Computations

Maximum Angular Excursions — Figure 3a shows the equilibrium static trim, magnification factor, and rolling trim for a locked-in condition ($p = \omega$). The static trim at booster separation, approximately 0.25 degree, decreases to 0.14 degree at Apache ignition. This decrease in α_{ST} reflects the decrease in

*See Appendix, Figures A-1 through A-14

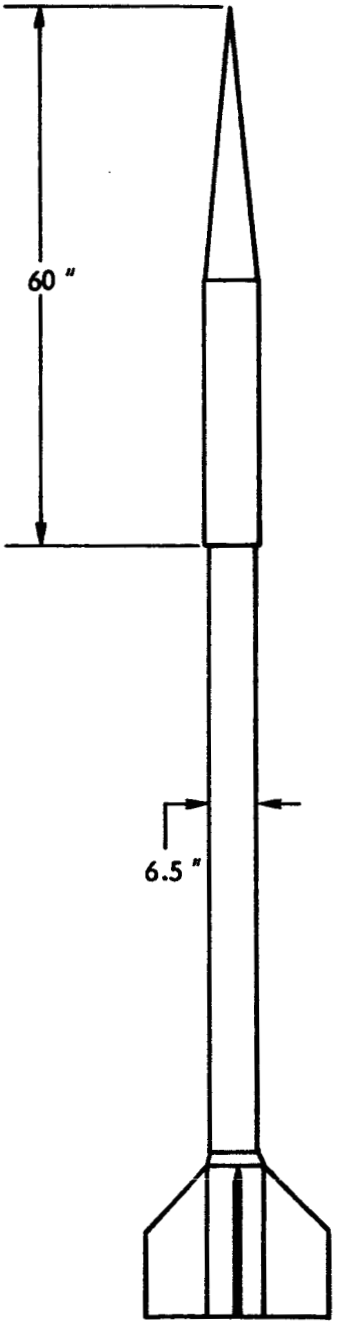

Figure 1. Apache Sounding Rocket, Study Model

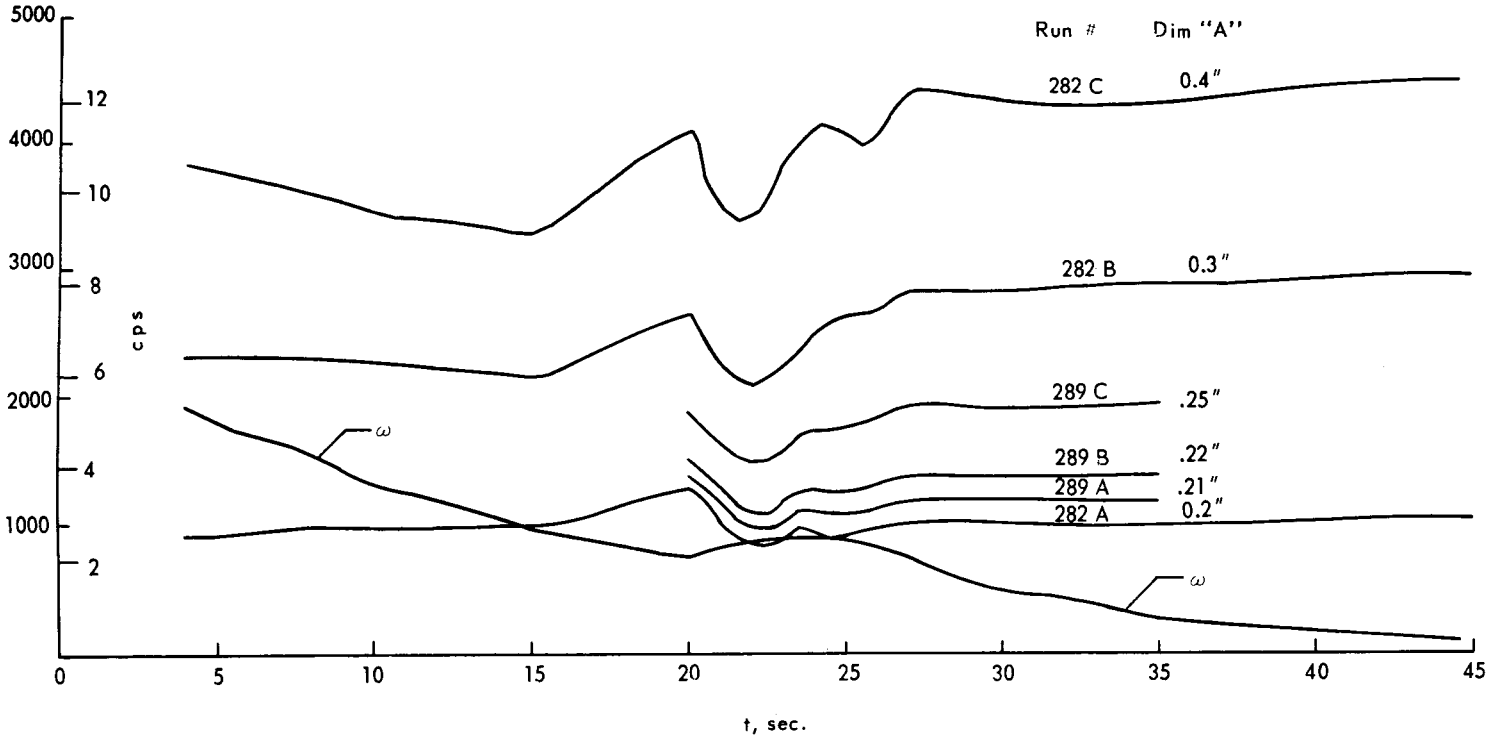

Figure 2. Histories, Roll and Undamped Pitch Rate

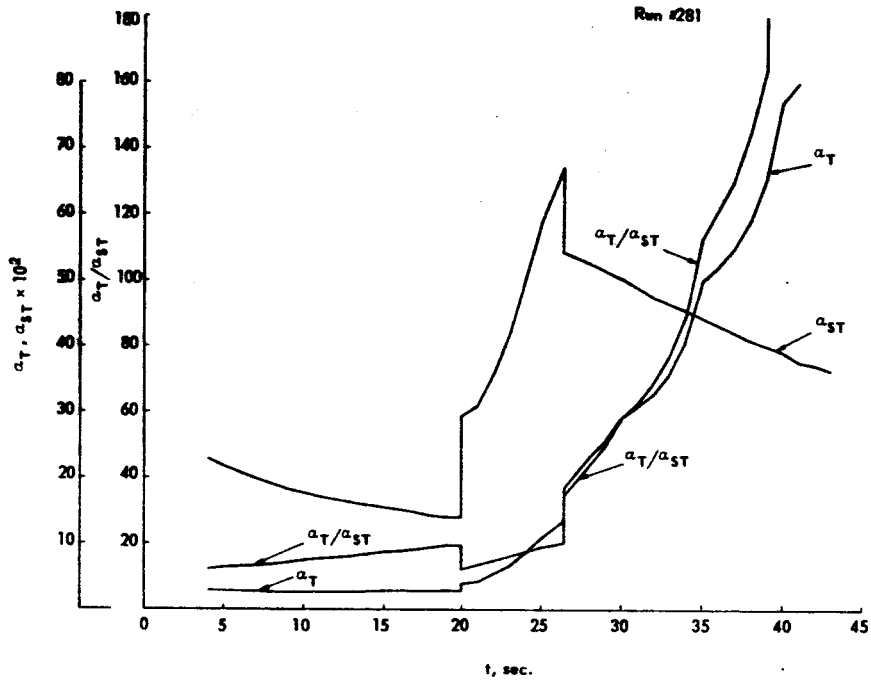

(a) t_{max} = 45 sec

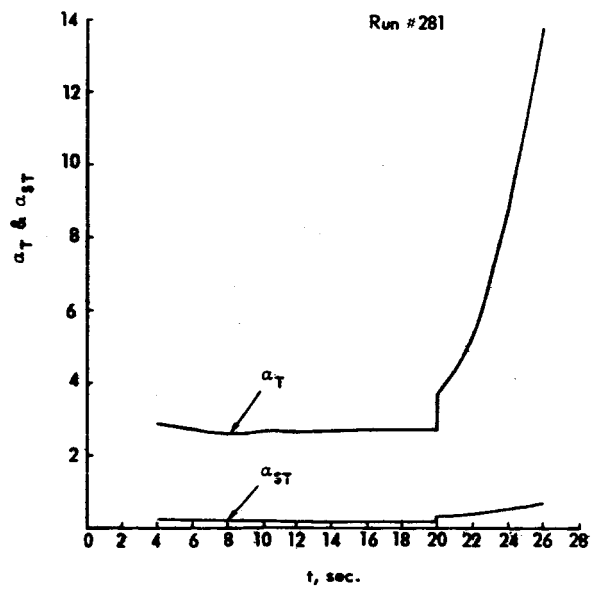

(b) $\alpha_{T_{max}}$ = 12 degrees

Figure 3. Static Trim, Magnification Factor, and Rolling Trim for Locked-In Condition

the Mach number from about 3 at booster separation to 1.8 at Apache ignition, causing an increase in $|C_{m_\alpha}|$. During Apache burn, α_{ST} increases from 0.29 degree to a maximum of 0.67 degree because of the rapid decrease in $|C_{m_\alpha}|$ compared to the dynamic pressure increase. At thrust termination, α_{ST} decreases to 0.54 degree and continues to decrease with increasing time (decreasing Mach number, increasing $|C_{m_\alpha}|$). Before Apache ignition, the magnification factor, α_T/α_{ST}, increases at about the same rate α_{ST} decreases, resulting in a nearly constant α_T of 2.5 degrees. This implies that lock-in after booster separation and before Apache ignition will not degrade flight performance provided that breakout occurs before Apache ignition. Interestingly, for the two flights that are documented (3, 12), lock-in did occur for a short interval before second-stage ignition with no measurable increase in angle-of-attack.

At Apache ignition, the magnification factor decreases from jet damping and axial acceleration effects; hence, α_T reflects only a small fraction of the α_{ST} increase. At Apache burnout, the magnification factor increases more than the static trim decreases and, hence, α_T increases. In other words, if the vehicle is locked in, then at Apache burnout a jump (increase) in angle-of-attack will occur. After burnout, α_T increases exponentially until the vehicle is in a flat spin.

Since the simulation program used in this study is limited to small angles, a program cutoff angle of 12 degrees was used for further studies. Figure 3(b) shows α_{ST} and α_T replotted for this upper limit. If the vehicle remains locked in until the angle-of-attack exceeds 12 degrees, breakout is not possible and the flight will have failed anyway.

Asymmetry Tolerances Before Apache Ignition — Figure 4 shows the effects of induced roll moments on the allowable center-of-gravity offsets for various tab settings. If, for example, dimension A in Figure 4(a) = 0.2 inch, then a center-of-gravity offset of 0.26 inch is sufficient to cause lock-in throughout the entire flight for the quadraloop-forward configuration, whereas 0.46 inch would be required for the clean configuration. As stated previously, the maximum allowable offset is the value at Apache ignition ($t = 20$ sec) which, in turn, is determined by the value of the undisturbed roll rate at Apache ignition. Hence, the shape of the undisturbed roll-rate curve after booster burnout and before Apache ignition determines the time interval the vehicle is locked in; whereas, the undisturbed peak roll rate at Apache ignition determines the allowable asymmetries. Since lock-in before Apache ignition and after Nike burnout does not degrade flight performance provided that breakout occurs before Apache ignition, Figure 5 shows the allowable tolerances as a function of peak roll rate at Apache ignition. Figure 5 indicates that the effects of the quadraloops in the forward position are significant only when the peak undisturbed roll rate is less than 4 cps. For

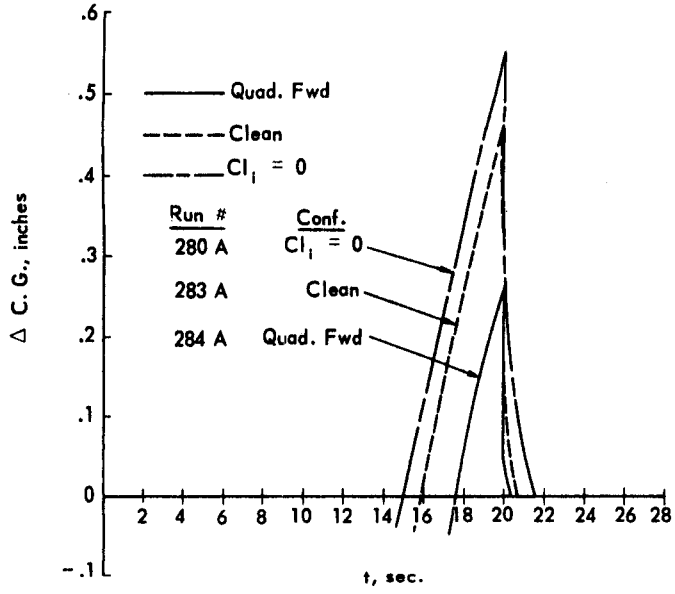

(a) A = 0.2 inches

GPL = 80 lb; payload length = 60 inches

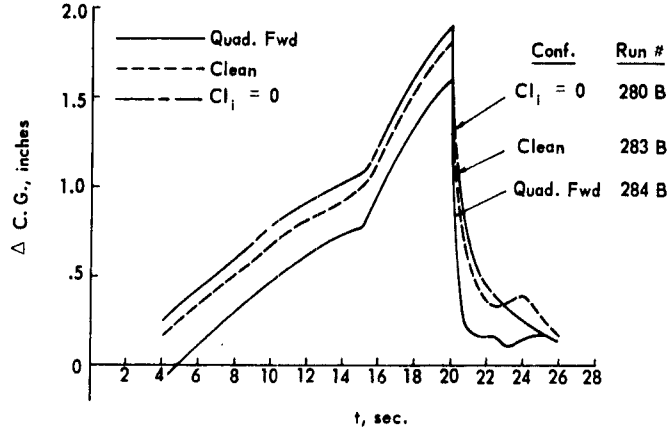

(b) A = 0.3 inches

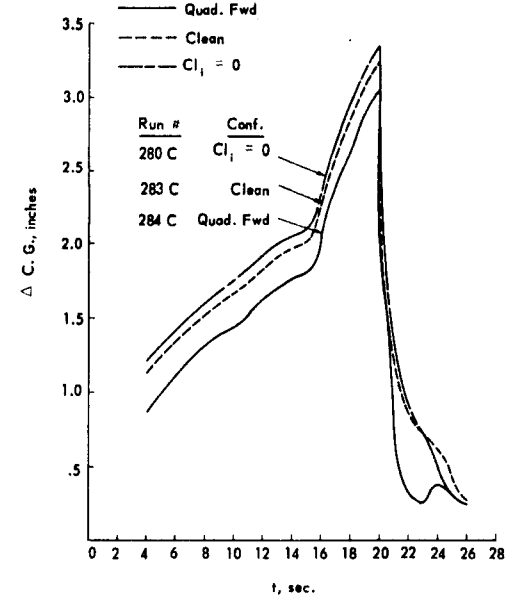

(c) A = 0.4 inches

Figure 4. Apache Center-of-Gravity Tolerance

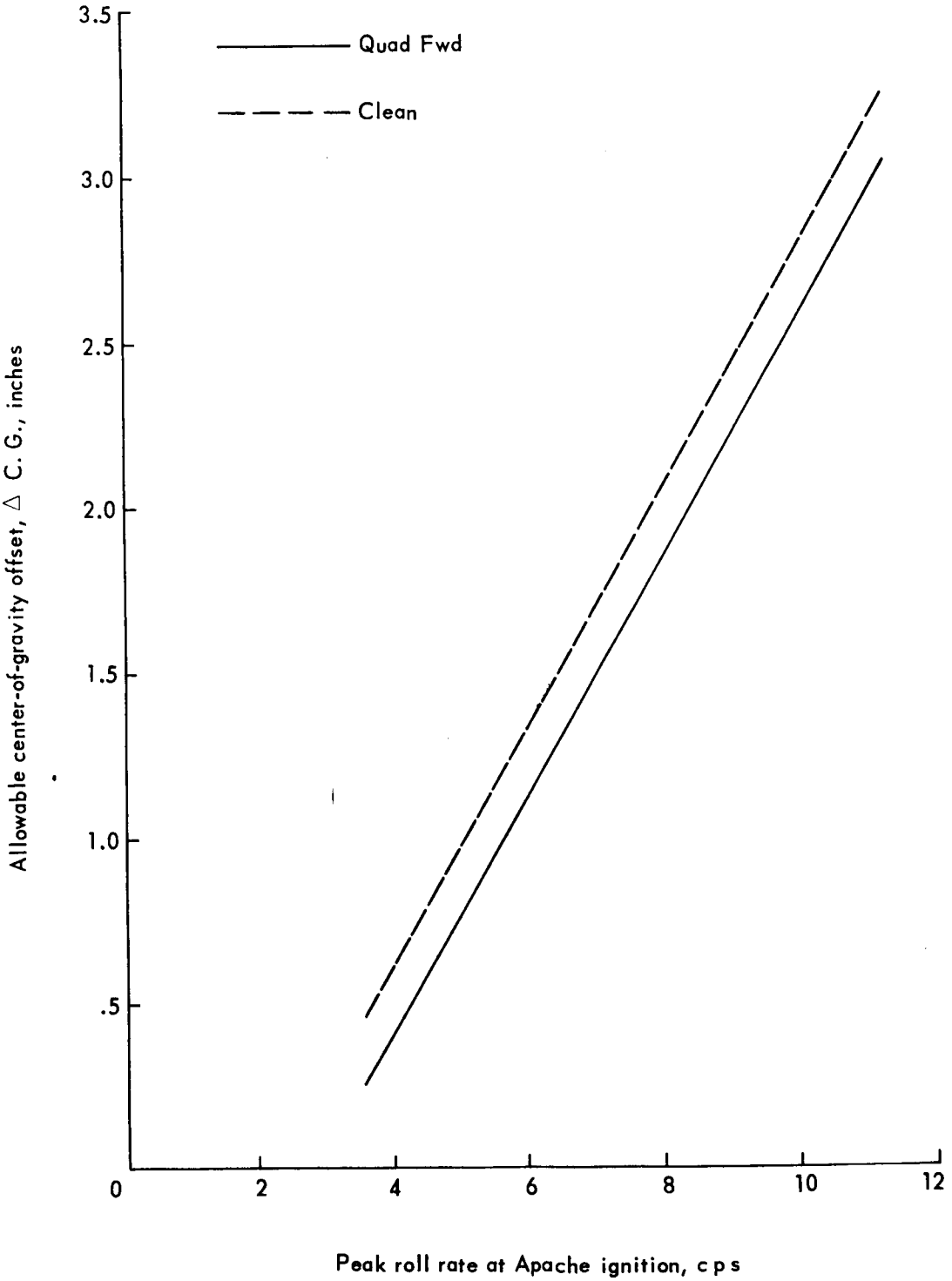

Figure 5. Center-of-Gravity Tolerance for Breaking Out of Lock-In Before Apache Ignition

conventional flight peak roll rates on the order of 8 to 10 cps, the allowable tolerances are much greater than conceivable values. (Reference 13 estimates the maximum center-of-gravity offset to be on the order of 0.07 inch.)

Asymmetry Tolerances During Apache Burning — As concluded above, the quadraloops in the forward position will not affect flight performance before Apache ignition for conventional undisturbed peak roll rates. From the wind-tunnel data (Figure A2), the quadraloop forward-position induced roll-moment coefficients diminish to zero by $t = 24.3$ seconds; thus, if the quadraloops affect flight performance at all, the disturbances must start after Apache ignition and before $t = 24.3$ seconds. Figure 6 shows the allowable center-of-gravity offset during this time interval. Figure 6 shows that, for an assumed $\Delta CG = 0.1$ inches, the clean configuration would require an undisturbed roll rate of about 1 cps above the natural frequency to break out of roll lock-in, whereas the quadraloops would require about 6 cps. The possibility of breaking out of lock-in is therefore greatly reduced when the quadraloops are in the forward position.

The foregoing discussion is based on the assumption that the vehicle is locked in during Apache burn. From earlier discussions, if conventional undisturbed peak roll rates prevail at Apache ignition the vehicle will not be locked in at Apache ignition. The values in Figure 6 are valid only if the undisturbed roll rate dips across the natural frequency curve, or comes close enough for capture. The next phase of study is to determine the minimum frequency increment allowable between the roll and undamped pitch frequencies during second-stage burn to avoid capture. Since the vehicle is not locked in before capture, the equilibrium worst-case solutions do not apply and dynamic simulations must be considered.

Dynamic Simulations

In order to get a feeling for the growth of α_T, trim orientation shift and the mechanism for capture, the equilibrium trim and trim orientation were computed for various $(p_u - \omega)$ and are presented in Figures 7 and 8. The rapid changes in α_T and ϕ occur for $(p_u - \omega) \lesssim 0.5$ cps. If a 1-cps minimum increment exists, then α_T is less than α_{ST} and the worst center-of-gravity offset orientation for $p = \omega$ is no longer considered undesirable. Similarly, for the quad-forward configuration, a trim orientation to give maximum $(-C_{l_i})$ for $p >> \omega$ would give maximum $(+C_{l_i})$ at $p = \omega$; for the clean configuration, a trim orientation to give maximum $(-C_{l_i})$ at $p >> \omega$ would also give maximum $(-C_{l_i})$ at $p = \omega$. Near minimum $p_u - \omega$ ($t = 22$ sec), for small angles-of-attack ($\alpha \lesssim 2°$), the maximum magnitude of roll-degradation coefficient is small and nearly the same value for center-of-gravity offset ($\Delta CG = 0.1$ in.) and induced roll-moment coefficient; whereas, at $\alpha = 6°$, the quad-forward configuration induced roll-moment coefficient is ten times the value attributed to center-of-gravity offset.

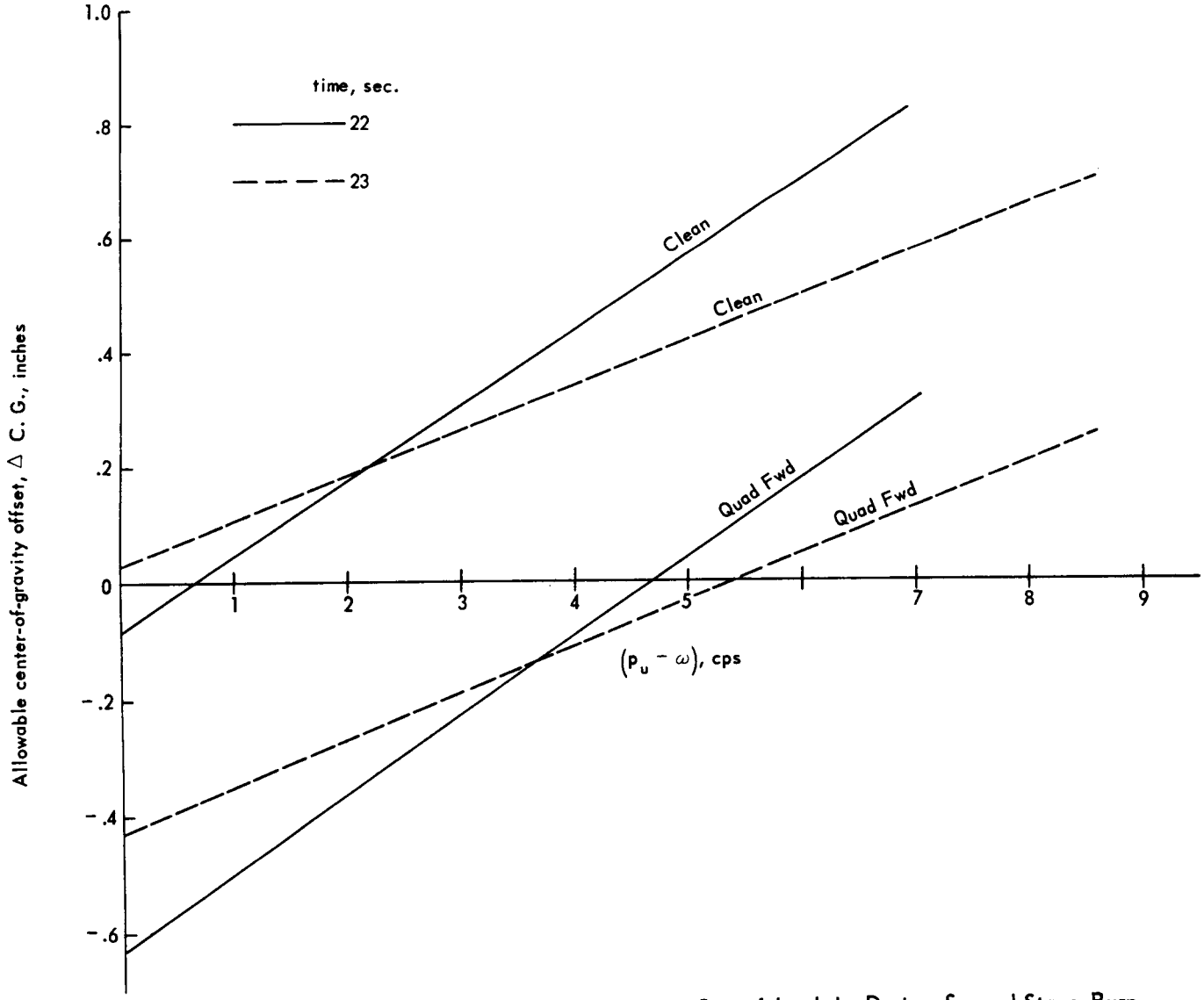

Figure 6. Center-of-Gravity Tolerance for Breaking Out of Lock-In During Second-Stage Burn

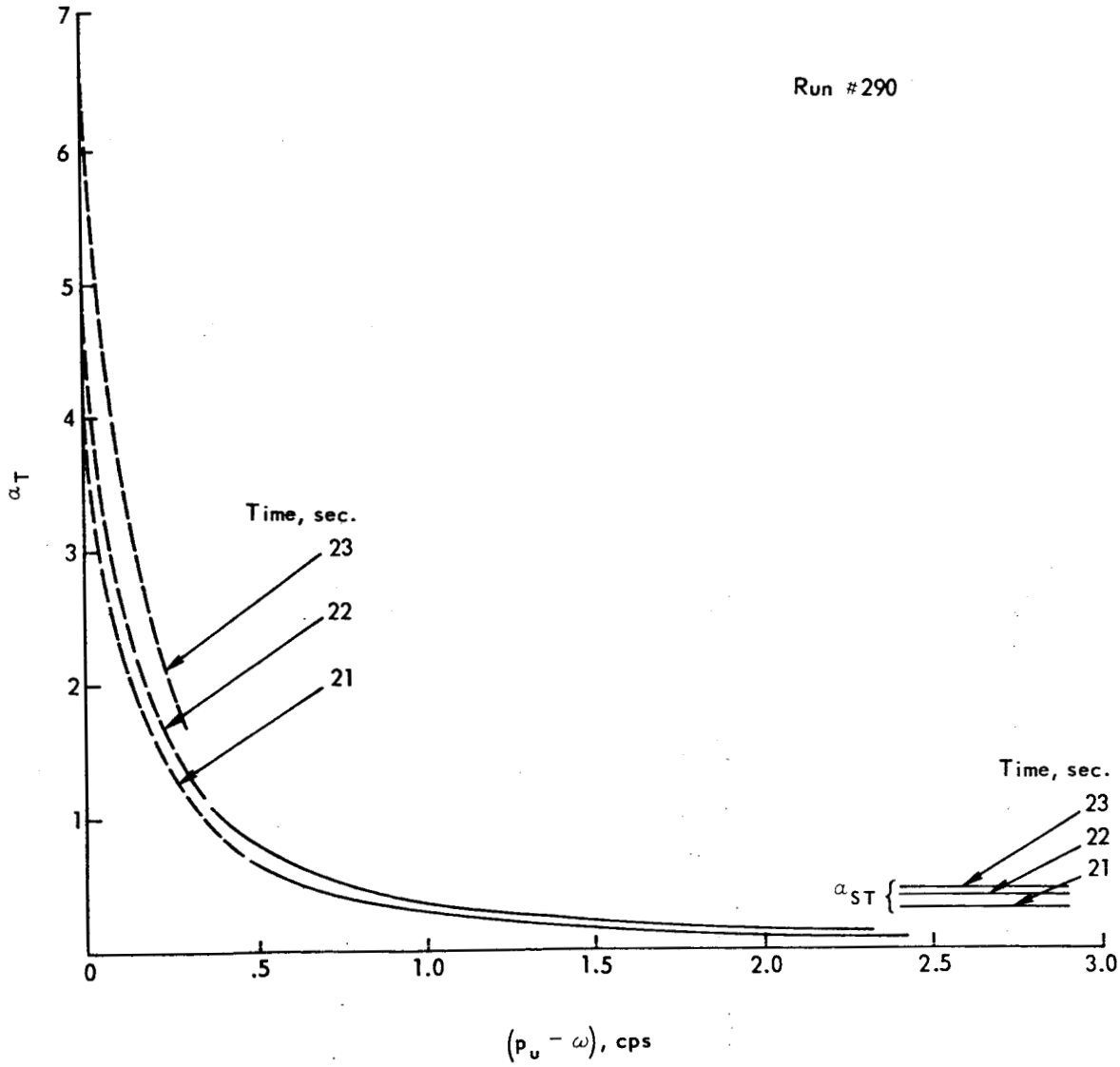

Figure 7. Rolling Trim During Second-Stage Burn

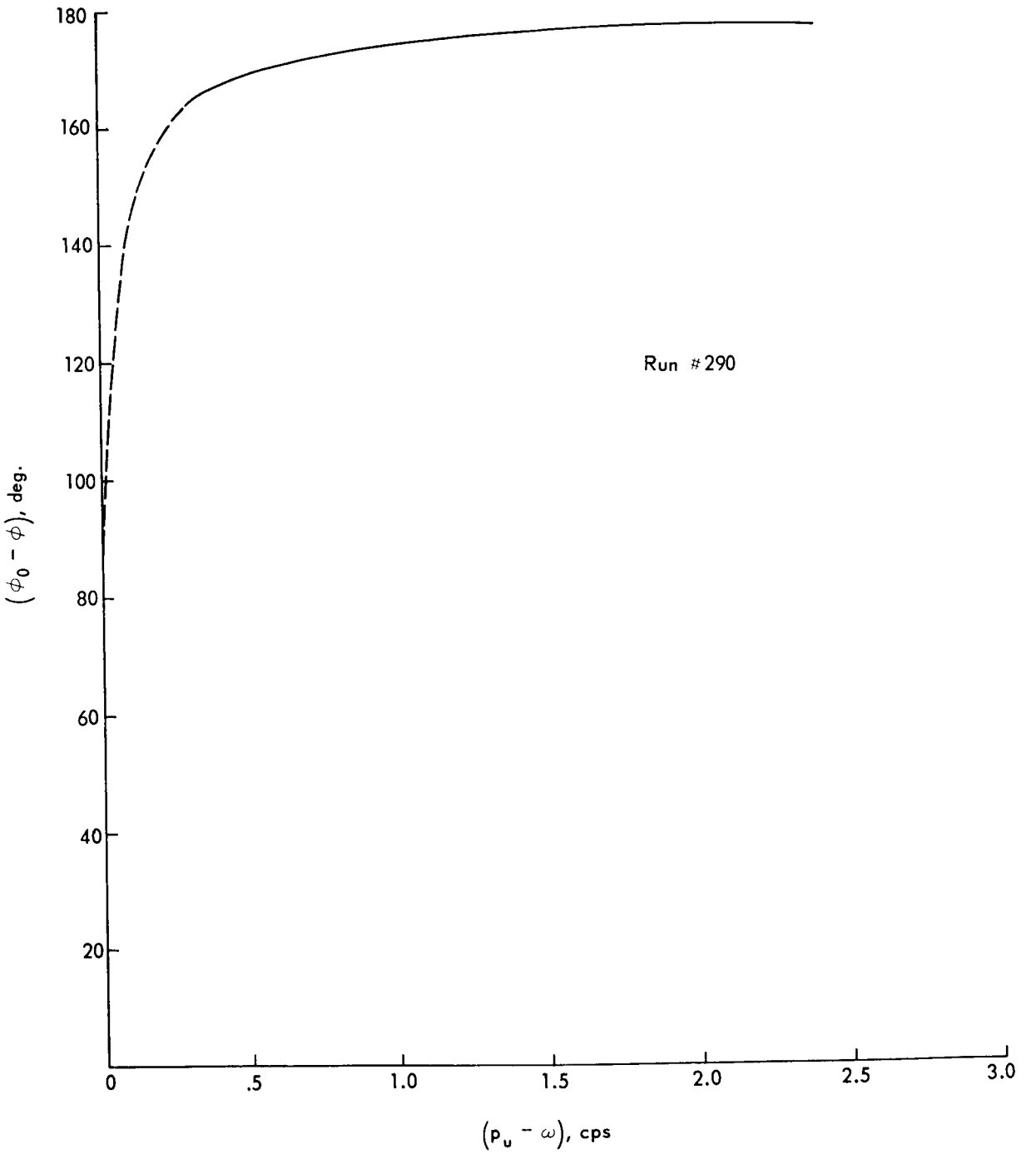

Figure 8. Trim Orientation During Second-Stage Burn

From the above discussion, three cases for capture were considered:

- Maximum $\left(-C_{l_i}\right)$ at minimum $(p_u - \omega)$

  Maximum $\left(-C_{N_\alpha} \alpha \frac{\Delta CG}{d}\right)$ at $p \approx \omega$

- Maximum $-C_{l_i}$ at $p \approx \omega$

  Maximum $\left(-C_{N_\alpha} \alpha \frac{\Delta CG}{d}\right)$ at minimum $(p_u - \omega)$

- Maximum $-C_{l_i}$ at minimum $(p_u - \omega)$

  Maximum $\left(-C_{N_\alpha} \alpha \frac{\Delta CG}{d}\right)$ at minimum $(p_u - \omega)$

As the roll periods for the quadraloop and clean configurations are π and $\pi/2$ respectively (Figure 9), the proper center-of-gravity orientations were calculated using roll-orientation dynamic lag effects obtained from dynamic runs with zero induced-roll moments. (Note that the initial conditions for the dynamic simulations are equilibrium values.) Figure 10 shows the results. As expected, the worst case occurs in the quad-forward configuration (runs 292 P, Q, and R) in which the trim is oriented for maximum degradation in roll at minimum $(p_u - \omega)$. From Figure 10(c), for $(p_u - \omega) = 0.28$, both the clean and the quad-forward configurations locked in and exceeded 12 degrees before $t = 30$ sec. For $(p_u - \omega) = 0.65$, an angle-of-attack of about 1 degree occurs; however, for $(p_u - \omega) = 1.72$, α_T is not perturbed by the induced roll moments and α_T is less than α_{ST}. Therefore $(p_u - \omega) = 1$ cps is sufficient to avoid capture.

CONCLUSIONS

Data from wind tunnel testing have been used in equilibrium solutions and dynamic simulations to assess the effects of forward-mounted quadraloop antennas on the pitch/roll coupling characteristics of the Apache. The most significant conclusions are:

1. Lock-in occurring after booster separation and before Apache ignition will not degrade flight performance, provided that breakout also occurs before Apache ignition.

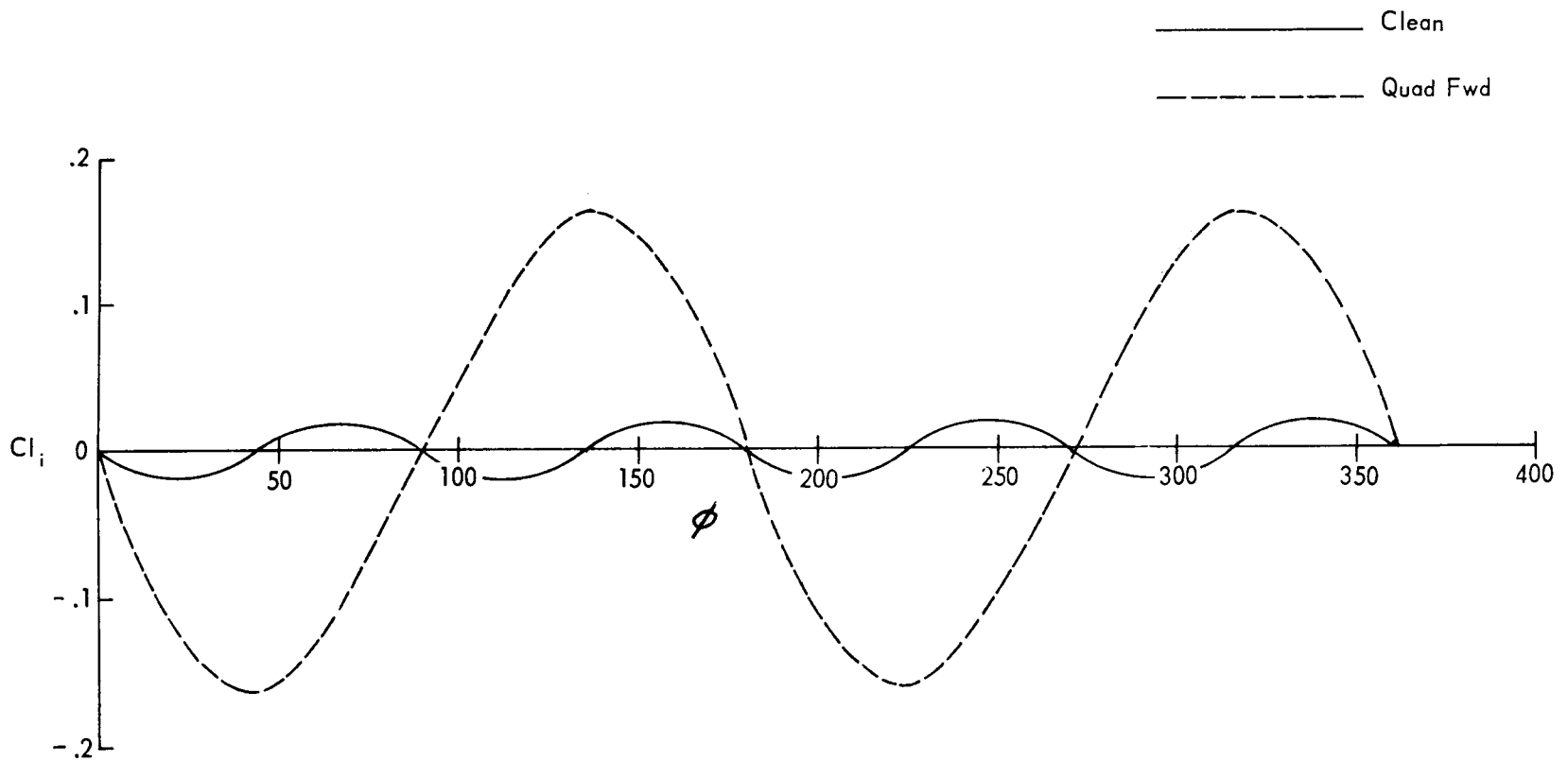

Figure 9. Induced Roll-Moment Coefficient at t = 21.8 Sec

$(\alpha_T)_{max}$, deg.				
Run No.	C_{l_i} \ $(p_u - \omega)^*$, cps	.28	.65	1.72
292 D, E, F	0	3.45	.66	.19
289 D, E, F	Clean	> 12.	.98	.21
292 G, H, I	Quad Fwd	> 12.	1.22	.22

*t = 22 sec.

(a) Maximum $\left(-C_{l_i}\right)$ at minimum $(p_u - \omega)$

Maximum $\left(-C_{N_\alpha}\alpha\frac{\Delta CG}{d}\right)$ at $p \approx \omega$

$(\alpha_T)_{max}$, deg.				
Run No.	C_{l_i} \ $(p_u - \omega)^*$, cps	.28	.65	1.72
292 J, K, L	0	> 12.	1.0	.22
289 G, H, I	Clean	> 12.	1.2	.22
292 M, N, O	Quad Fwd	2.92	0.78	.21

*t = 22 sec.

(b) Maximum $\left(-C_{l_i}\right)$ at $p \approx \omega$

Maximum $\left(-C_{N_\alpha}\alpha\frac{\Delta CG}{d}\right)$ at minimum $(p_u - \omega)$

$(\alpha_T)_{max}$, deg.				
Run No.	C_{l_i} \ $(p_u - \omega)^*$, cps	.28	.65	1.72
292 J, K, L	0	> 12.	1.0	.22
289 J, K, L	Clean	> 12.	.73	.21
292 P, Q, R	Quad Fwd	> 12.	1.54	.22

*t = 22 sec.

(c) Maximum $\left(-C_{l_i}\right)$ at minimum $(p_u - \omega)$

Maximum $\left(-C_{N_\alpha}\alpha\frac{\Delta CG}{d}\right)$ at minimum $(p_u - \omega)$

Figure 10. Results of Dynamic Simulation Cases (ΔCG = 0.1 in)

2. If the vehicle is locked in, then a jump (increase) in angle-of-attack will occur at Apache burnout owing to loss of jet damping and axial acceleration. After burnout, α_T increases until the vehicle is in a flat spin.

3. The success or failure of a flight depends upon the peak roll rate at Apache ignition, and upon the minimum frequency increment between the roll and undamped pitch frequencies during second-stage burn.

4. Before Apache ignition, the allowable asymmetries are much greater than conceivable for conventional-flight peak roll rates, on the order of 8 to 10 cps.

5. Having the quadraloops in the forward position greatly reduces the possibility of breaking out of lock-in during second-stage burn.

6. During second-stage burn, $(p_u - \omega) > 1$ cps is sufficient to avoid capture.

7. Consideration must be given to the increased loading and the loss in stability associated with the antenna elements. For the quadraloop configurations tested, antenna loading was a maximum of 60 percent of the lift provided by the clean body alone, and the loss in stability was about 1 caliber.

The only roll-setting requirement for a successful flight is that the peak roll rate at Apache ignition must be set high enough to maintain a minimum of at least 1 cps increment between the undisturbed roll and undamped pitch frequencies during Apache burn.

REFERENCES

1. Hawks, Roger J.: A Theoretical Investigation of the Rolling Motion of the Nike Cajun and Nike Apache Rocket Vehicles. GSFC X-721-65-335. August 1965.

2. Calfee, Dewey E.: Roll Speed-Up Analysis for High Altitude Sounding Rockets. ATL-TR-64-76. November 1964.

3. Galloway, Howard L., Jr.: The Effect of a Fin Trailing-Edge Wedge on the Roll History of a Nike Apache. GSFC X-721-66-85.

4. Memo of 19 June 1964, C. M. Hendricks to Files, Subject: Nike Apache Roll History

5. Memo of 22 July 1965, Edward E. Mayo to Distribution List, Subject: Antenna and Payload-Recovery Wind Tunnel Test Plans

6. Price, D. A., and Nelson, E. O.: Final Report for the Aerobee 150A Roll Lock-In Study. Contract No. NAS 5-9061, LMSC, Palo Alto, California. March 1965

7. Price, D. A., and Nelson, E. O.: Final Report for the Aerobee 350 Roll Lock-In Study. Extension to Contract No. NAS 5-9061, LMSC, Palo Alto, California

8. McNeal, D. R.: Description and Users Manual for Roll-Pitch Motion Digital Computer Program. LMSC Report No. M-60-64-2, LMSC, Palo Alto, California. March 1965

9. Memo of 8 February 1966, James S. Barrowman to Flight Performance Section Files, Subject: Lockheed RPM2 Program Usage

10. Memo of 25 April 1966, James S. Barrowman to Flight Performance Section Files, Subject: Memo to Flight Performance Section Files on Lockheed RPM2 Program Usage, dated 8 February 1966

11. Rocket and Recovery Systems Division 9324: Aeroballistic Design and Flight Results of the Sandia Nike Apache Rocket System (U). SC-4773(RR). April 1966

12. Sterhardt, J. A.: Environmental Test of Nike Apache Rocket NASA 14.111 GT. GSFC X-671-65-236. June 1965

13. Memo of 10 April 1964, D. J. Hershfield, Test and Evaluation Division, OTS to R. C. Baumann, Spacecraft Integration and Sounding Rocket Division, SS&SA, Subject: Principal Axis Tilt (PAT) of Apache and Payload

14. Thomas, C. G.: Investigation of a 0.410 Scale Model of a Cajun Rocket with Various Antenna Arrangements at Mach Numbers from 2.3 to 4.63. Fairchild Hiller Report. To be published

15. Mayo, Edward E.: Effects of Payload Weight and Length on the Mass and Aerodynamic Characteristics of the Apache and Cajun Sounding Rockets (Capache). GSFC X-721-66-91. March 1966

16. Mayo, Edward E.: Apache Notes (unpublished)

17. Memo of 15 September 1964, Roger J. Hawks to Howard L. Galloway, Subject: Nike-Capache Roll History

APPENDIX

APACHE INPUT DATA

Ref. 5

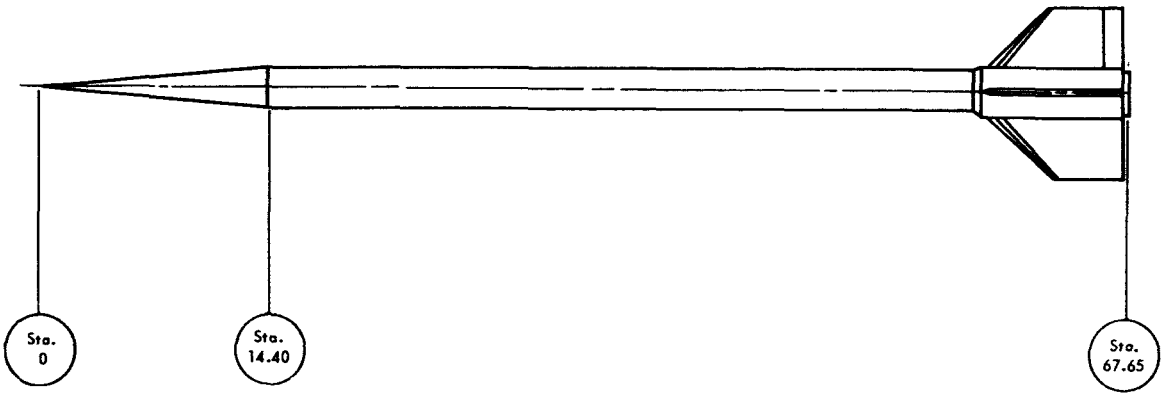

(a) Clean Configuration

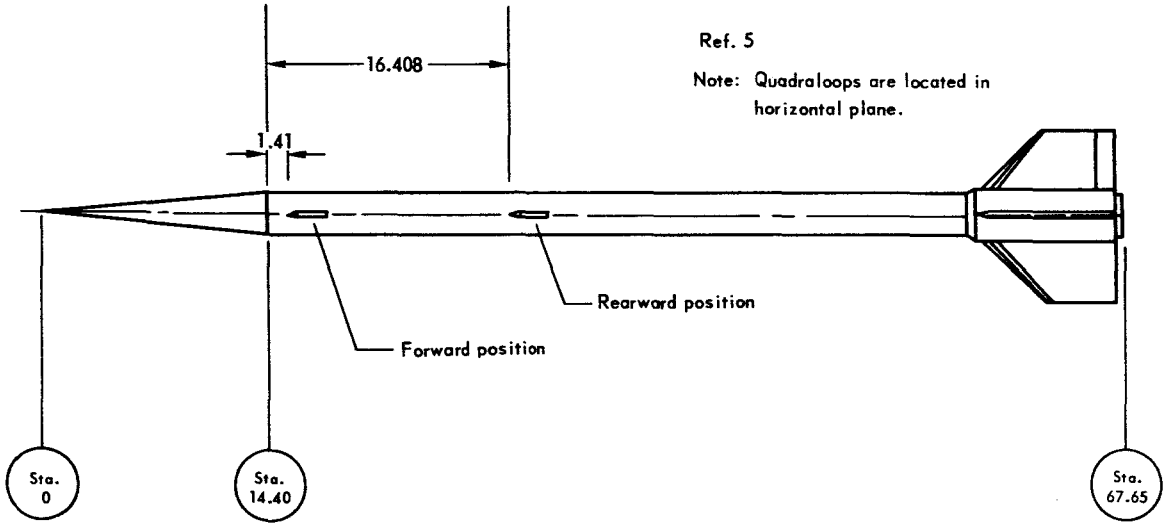

(b) Quadraloop Configuration

Ref. 5

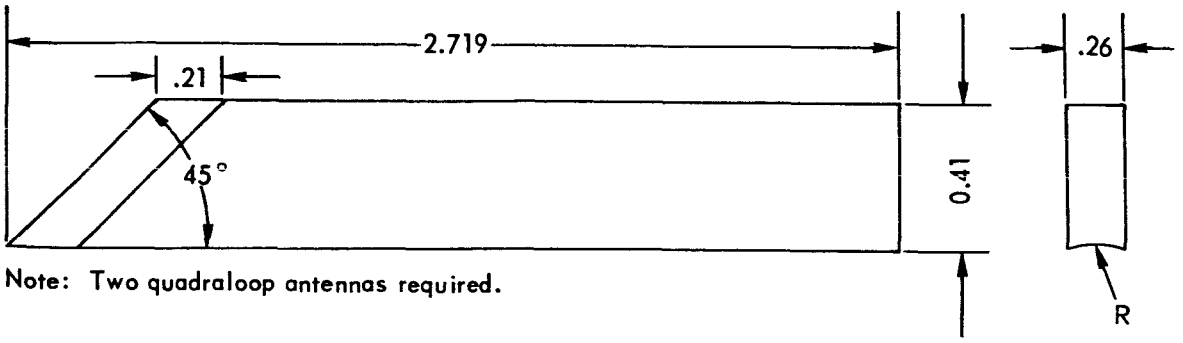

Note: Two quadraloop antennas required.

(c) Quadraloop Antenna

(All dimensions in inches)

Figure A-1. LUPWT Model Geometry

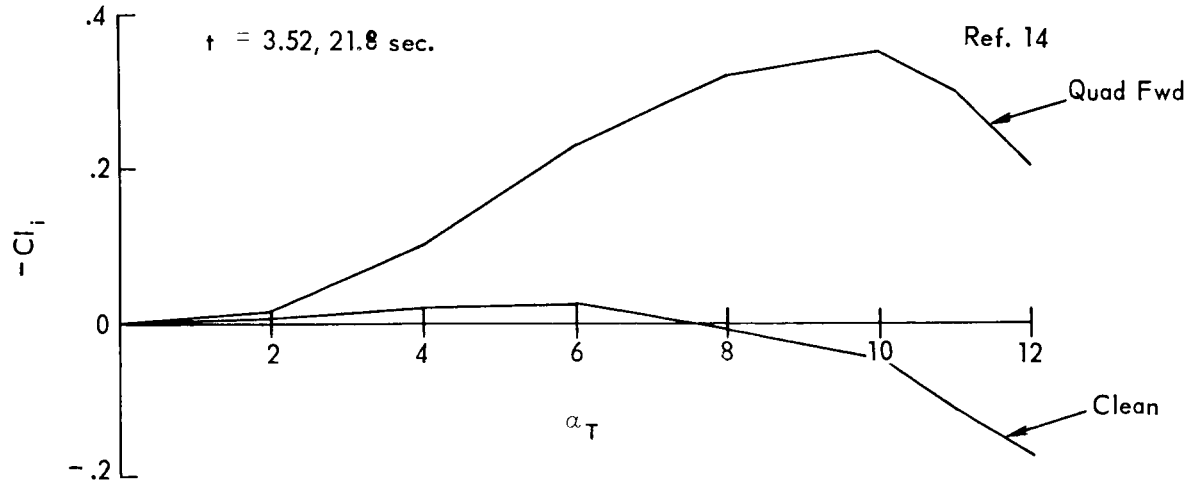

(a) M = 2.95

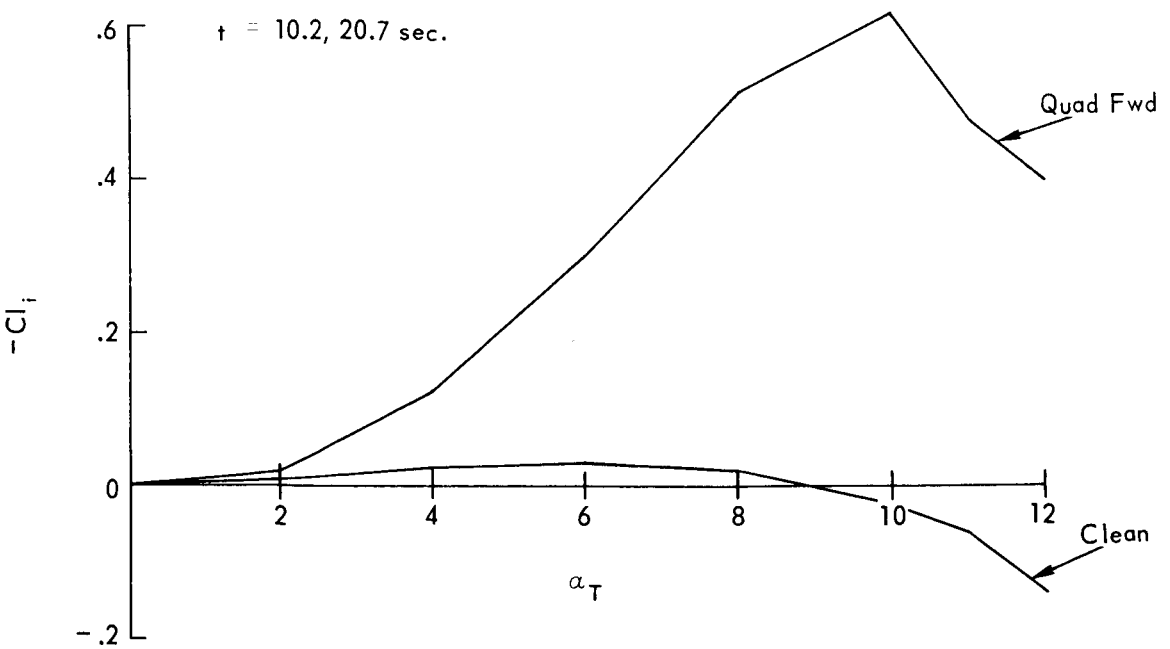

(b) M = 2.25

Figure A-2. Comparison of Induced Roll Moments for Clean and Quadraloop-Forward Position Configurations

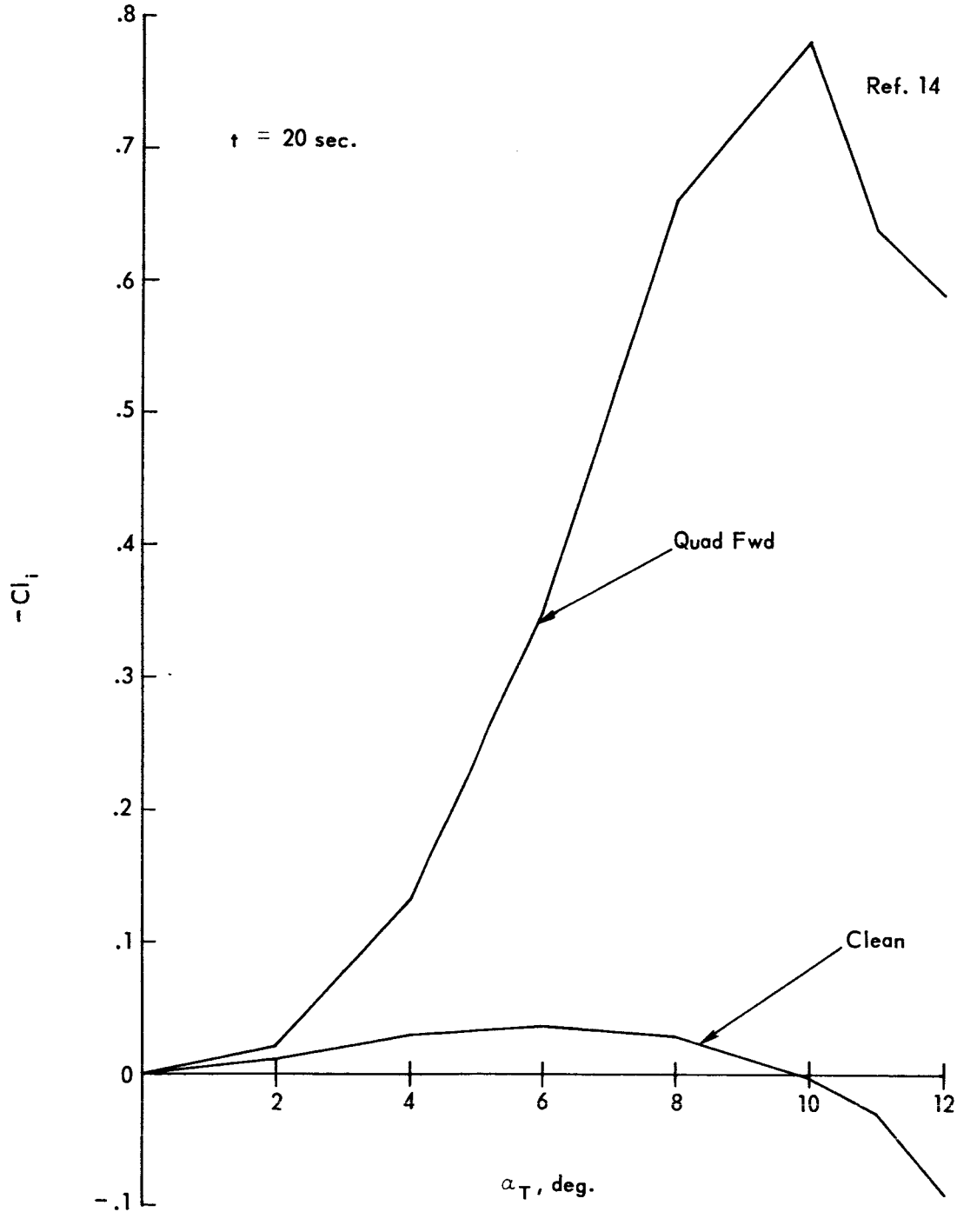

(c) M = 1.18

Figure A-2. Comparison of Induced Roll Moments for Clean and Quadraloop-Forward Position Configurations (Cont'd)

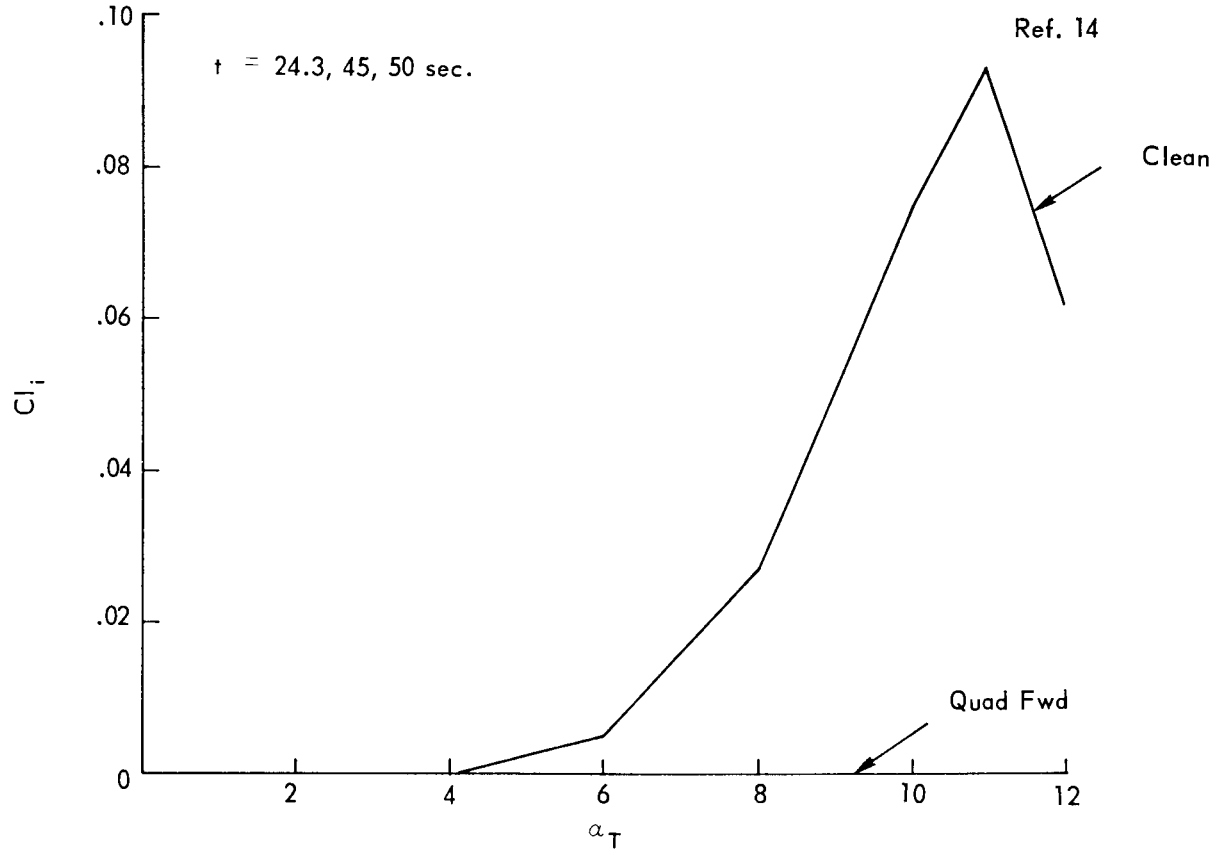

(d) M = 4.75

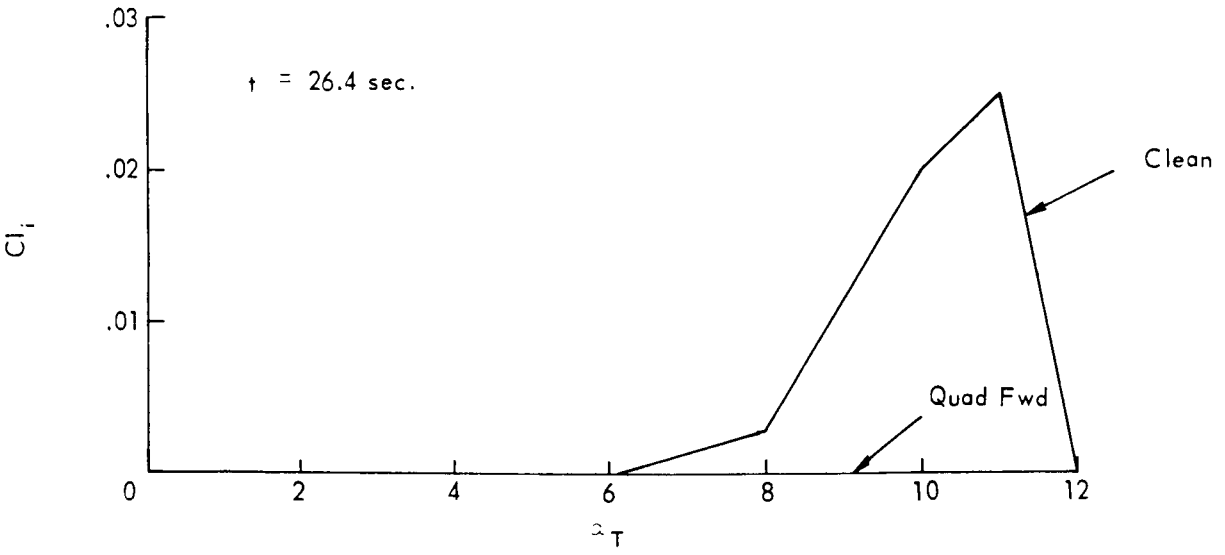

(e) M = 6.2

Figure A-2. Comparison of Induced Roll Moments for Clean and Quadraloop-Forward Position Configurations (Cont'd)

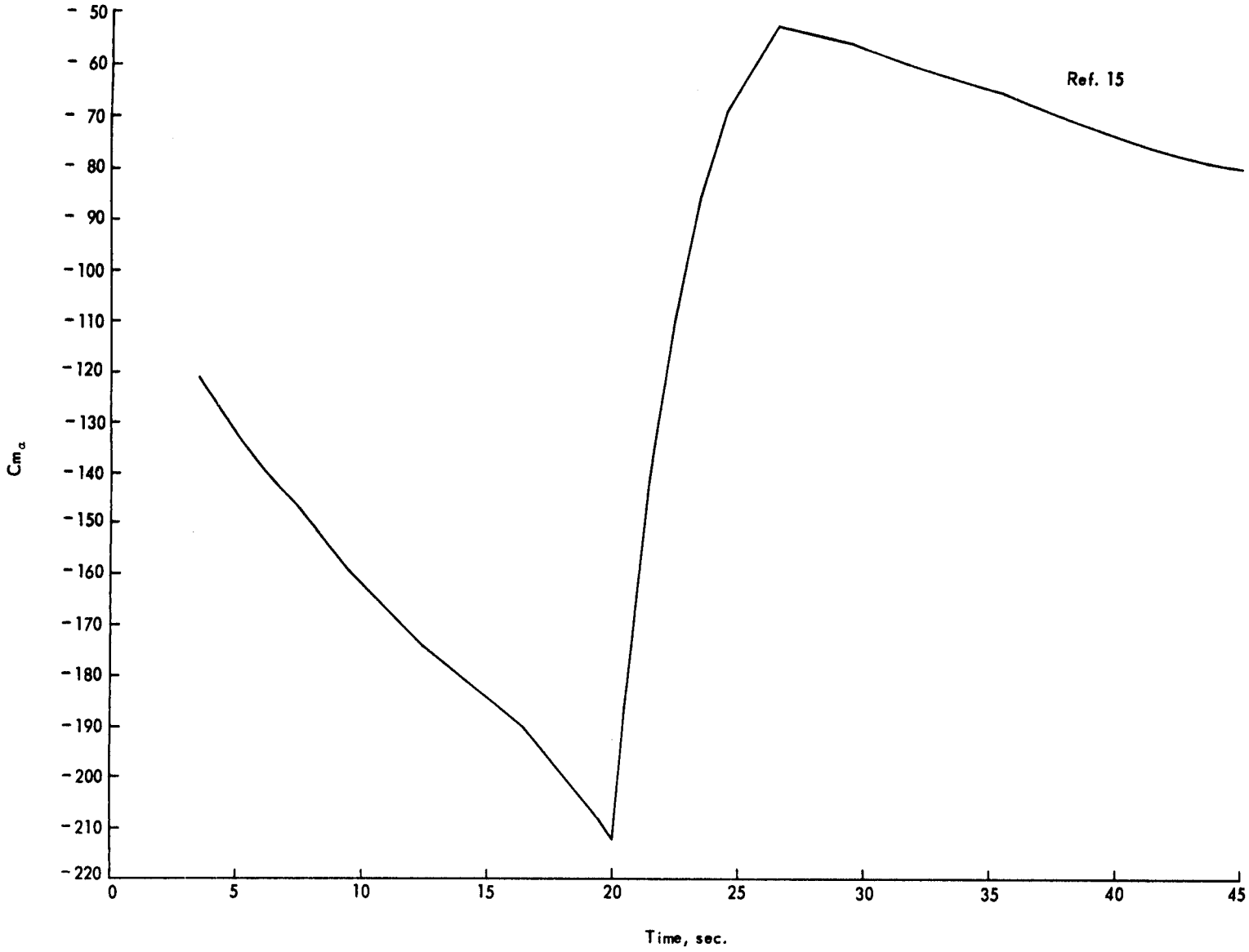

Figure A-3. Static Stability

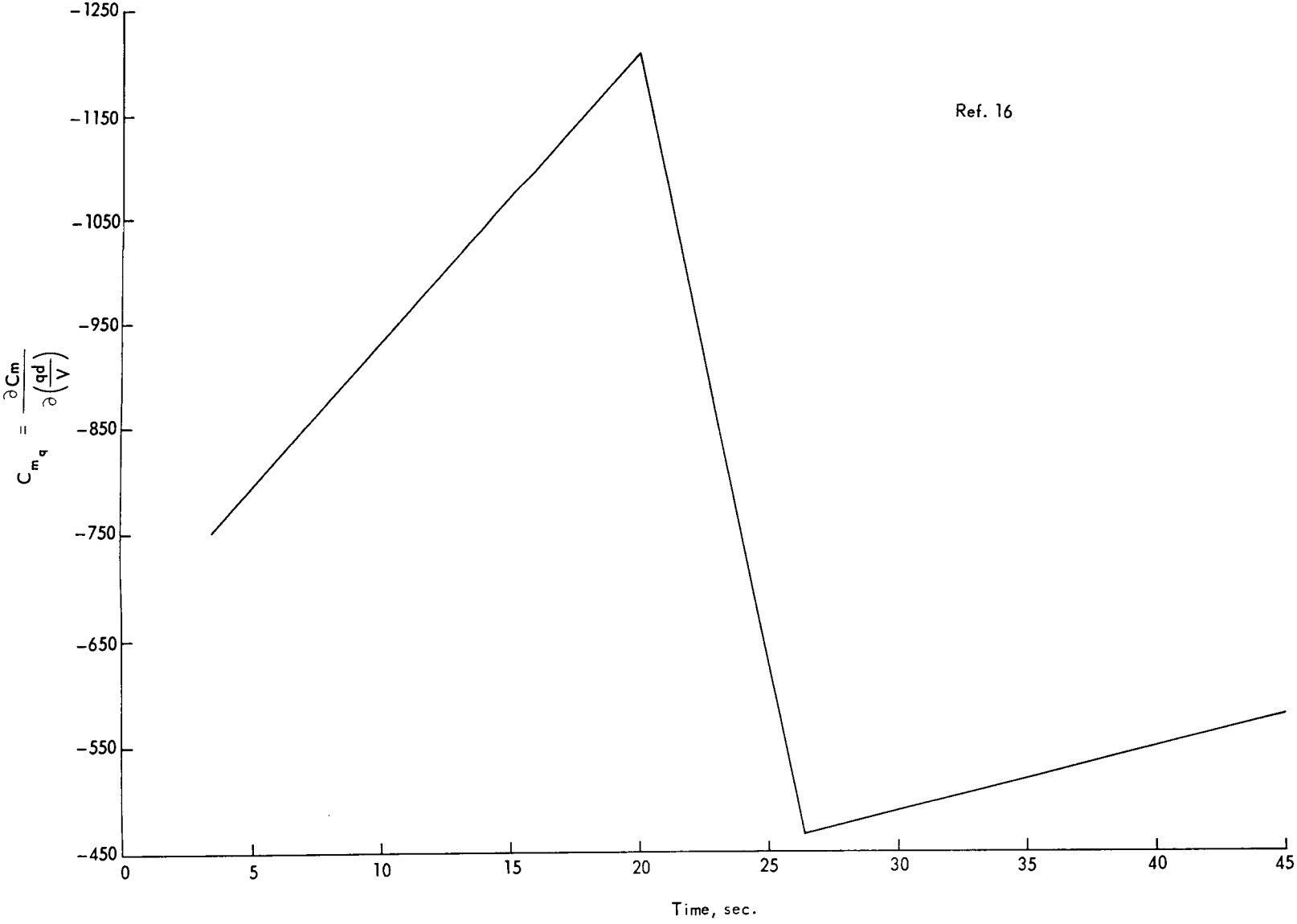

Figure A-4. Aerodynamic Pitch-Damping Coefficient

Ref. 16

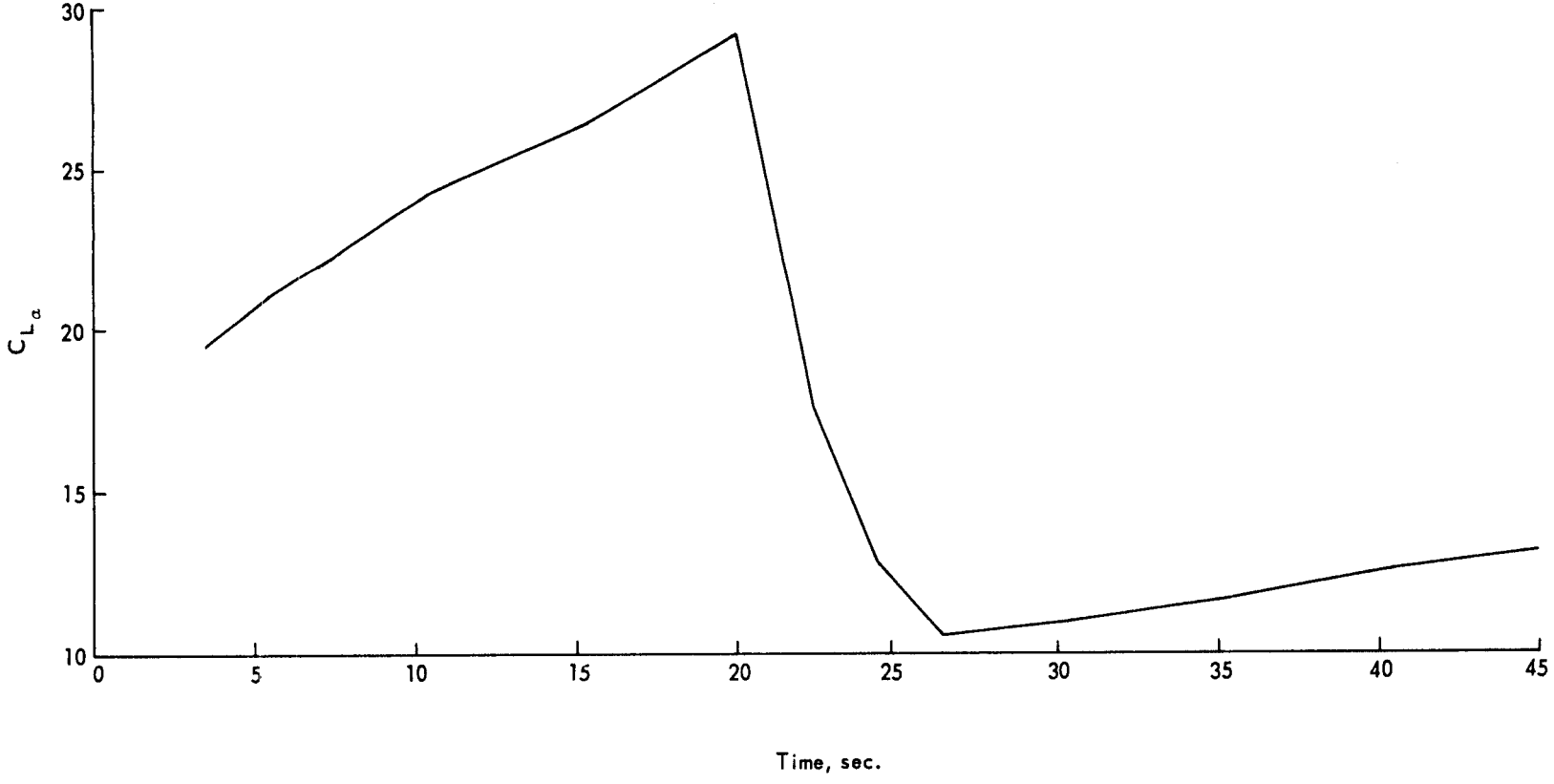

Figure A-5. Slope of Lift Curve

Ref. 16

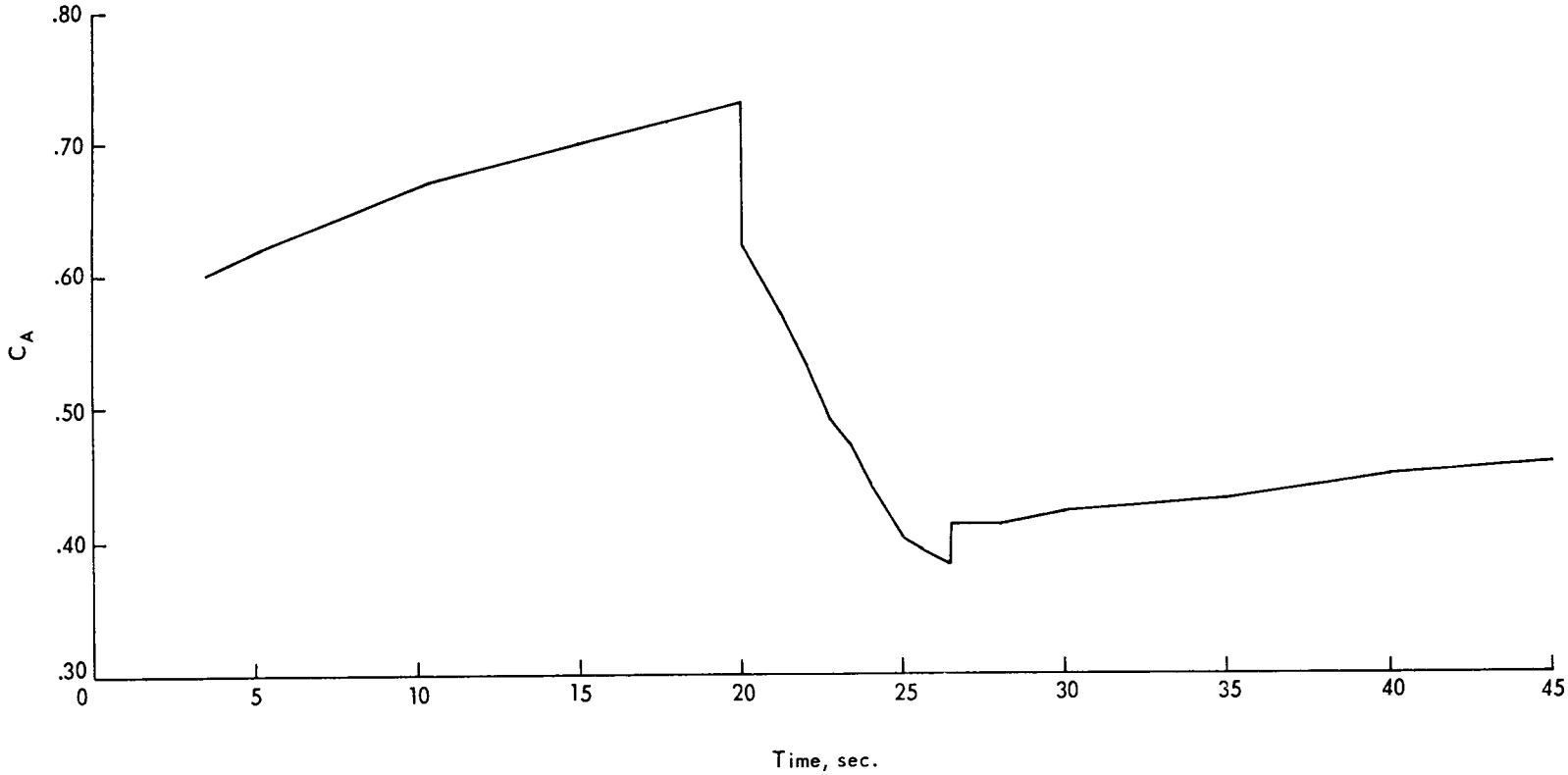

Figure A-6. Axial Force Coefficient

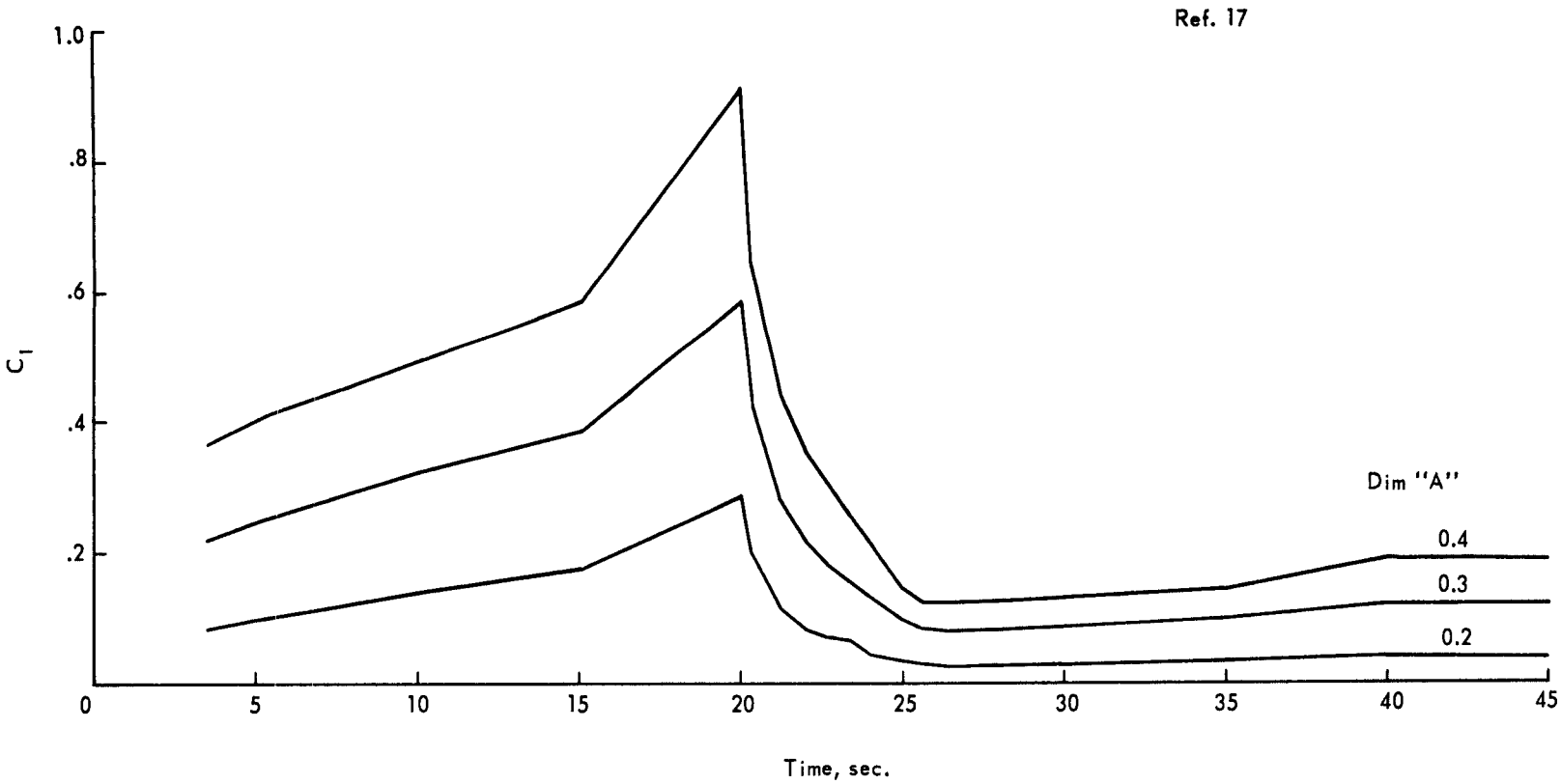

Figure A-7. Roll-Forcing Coefficient

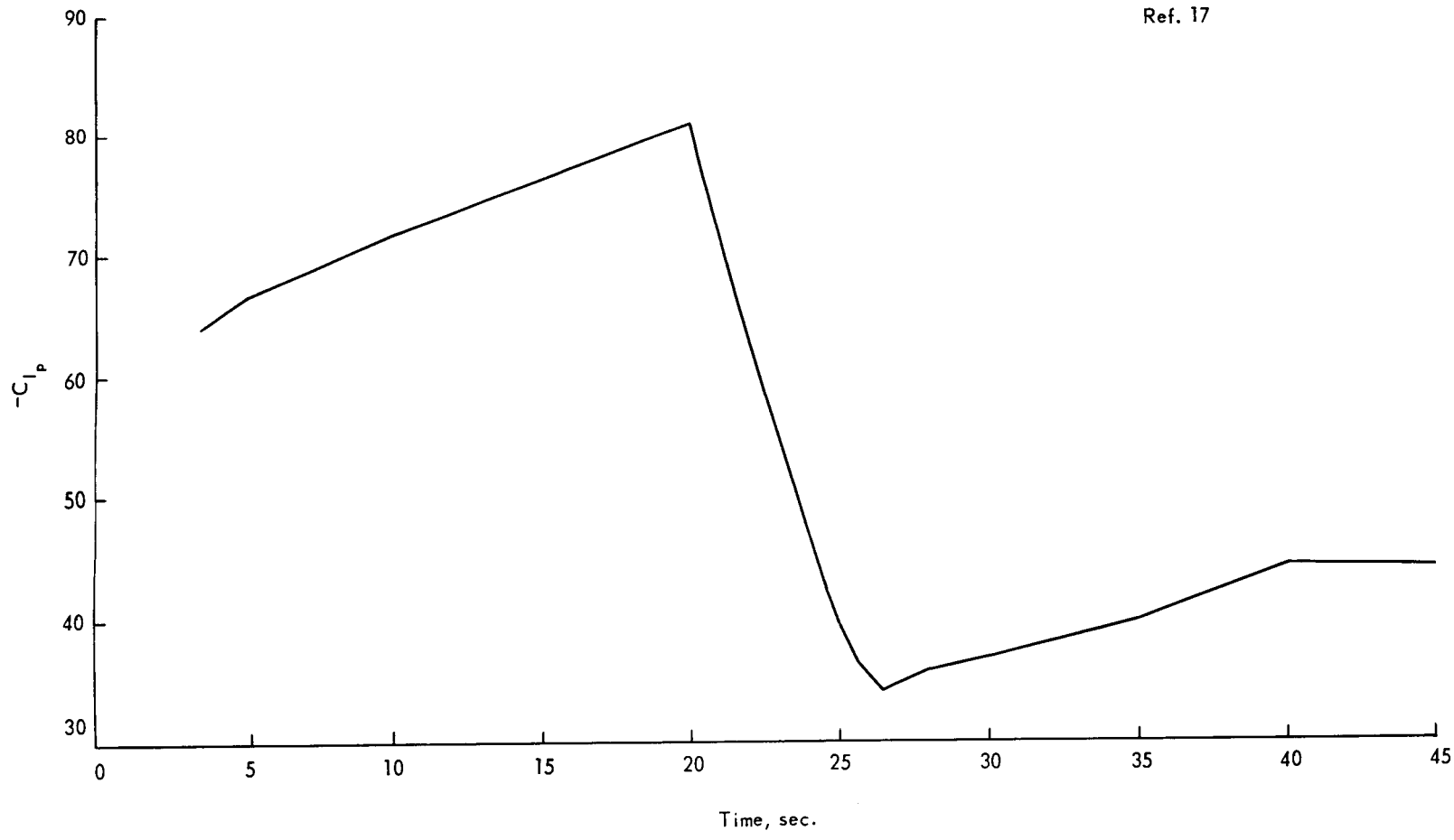

Figure A-8. Roll-Damping Coefficient

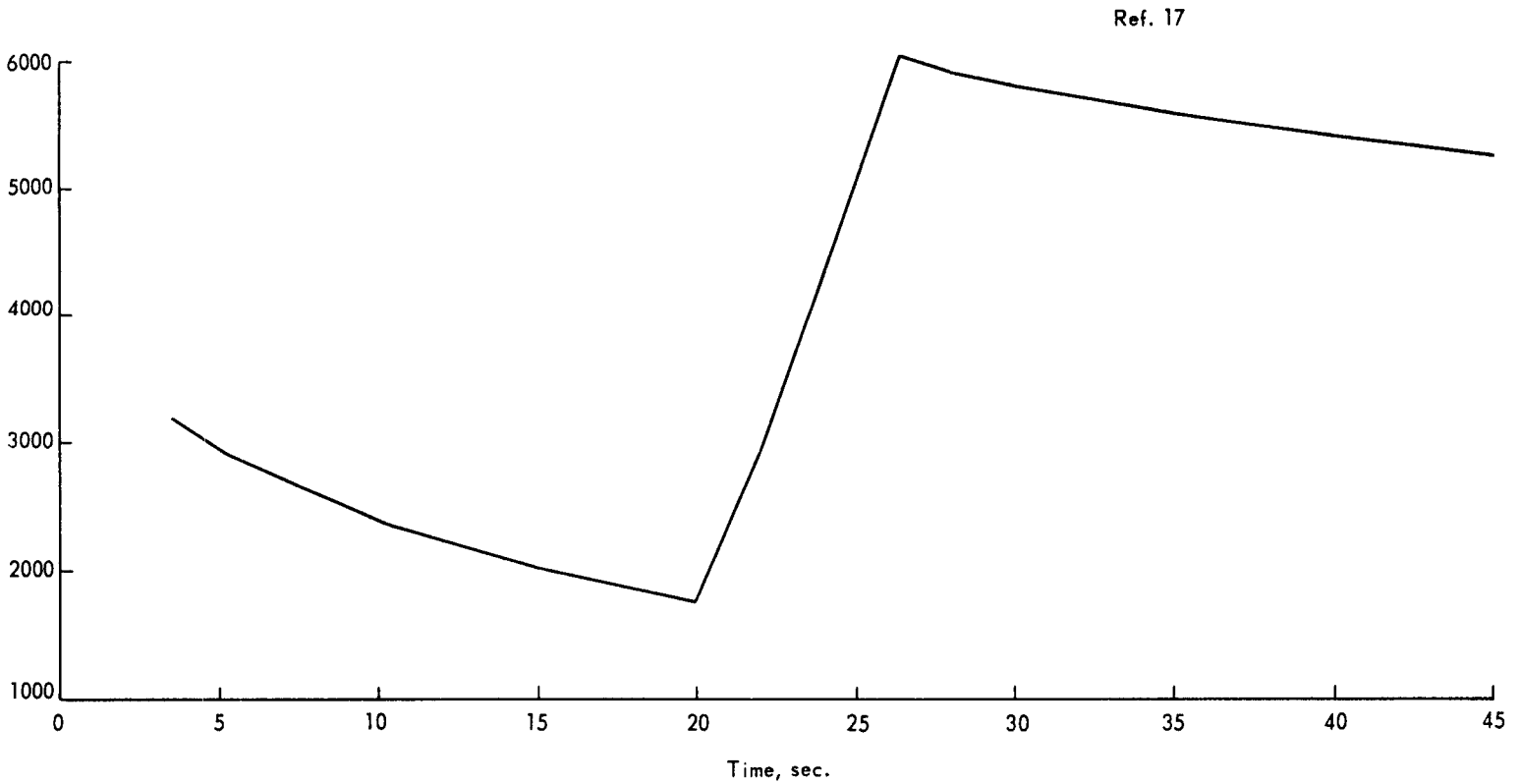

Figure A-9. Velocity History

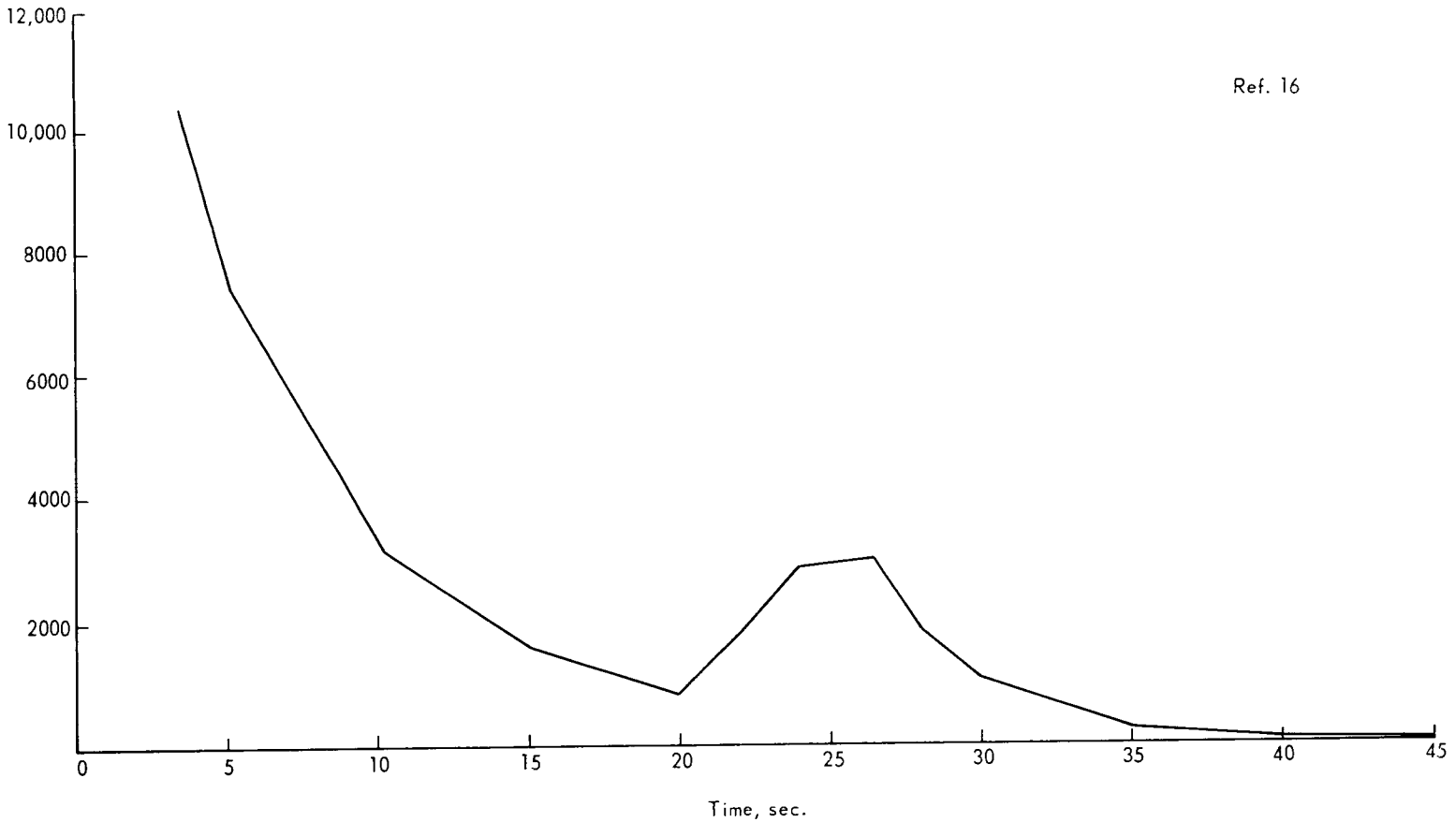

Figure A-10. Dynamic Pressure History

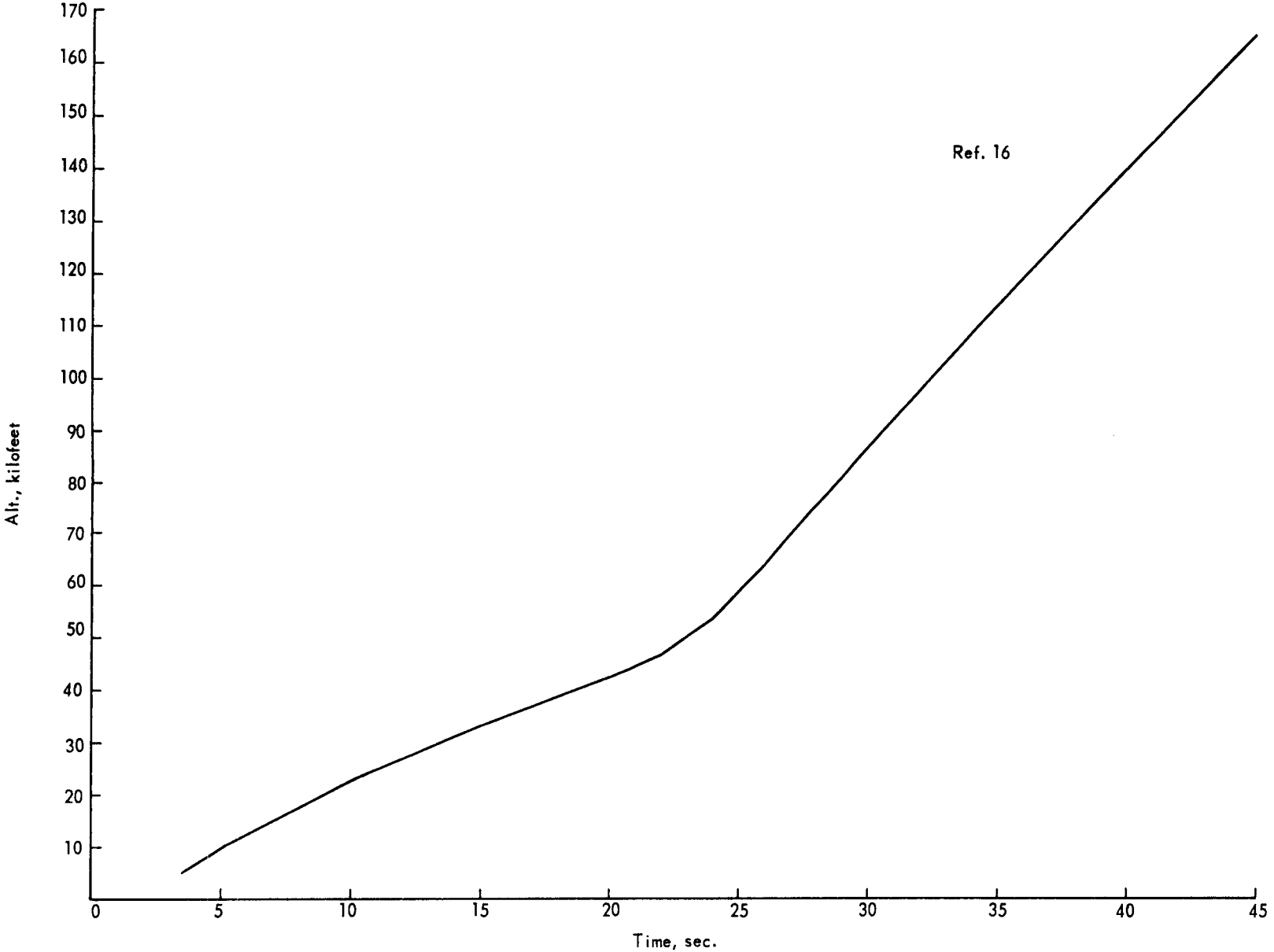

Figure A-11. Altitude History

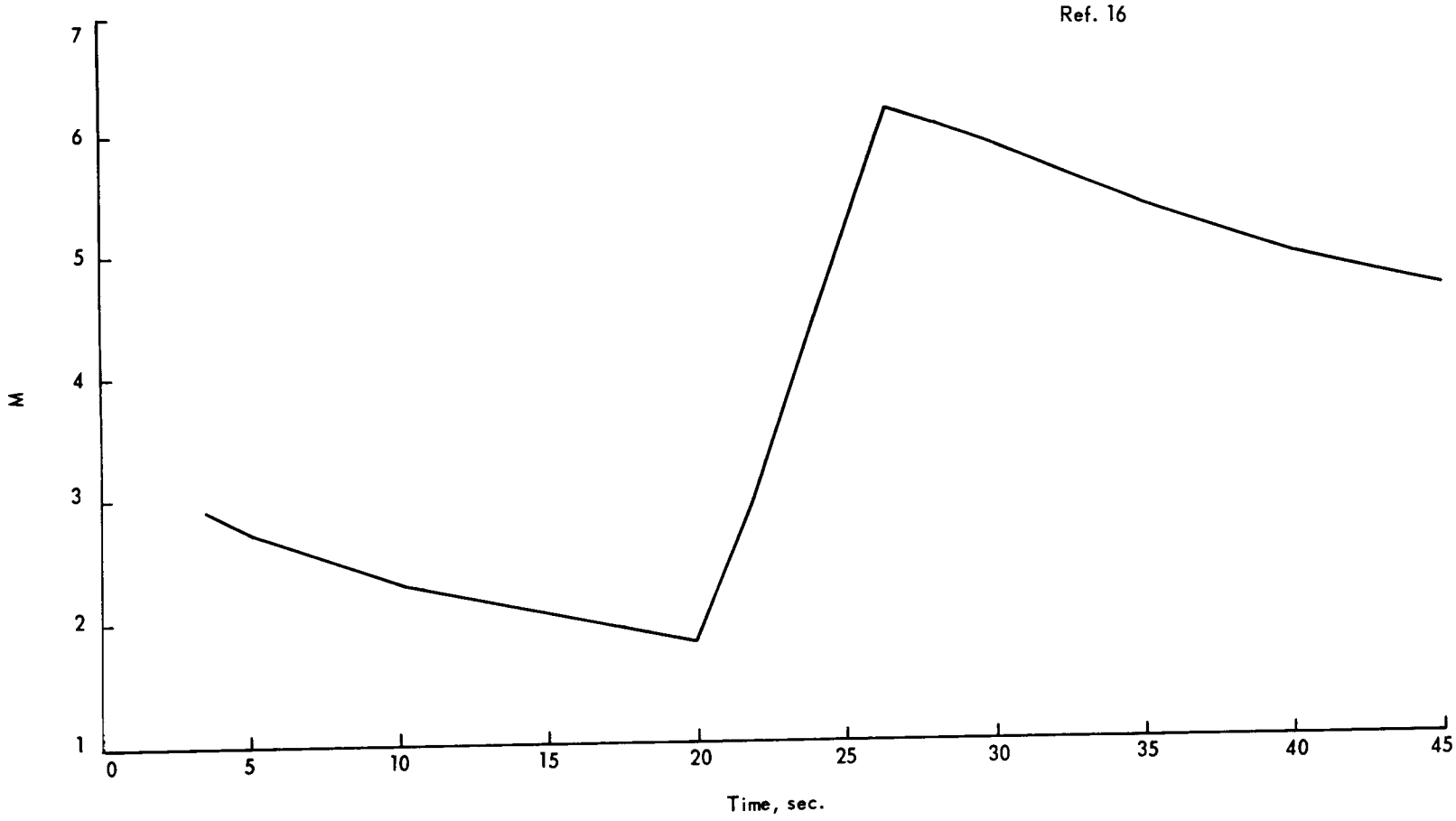

Figure A-12. Mach Number History

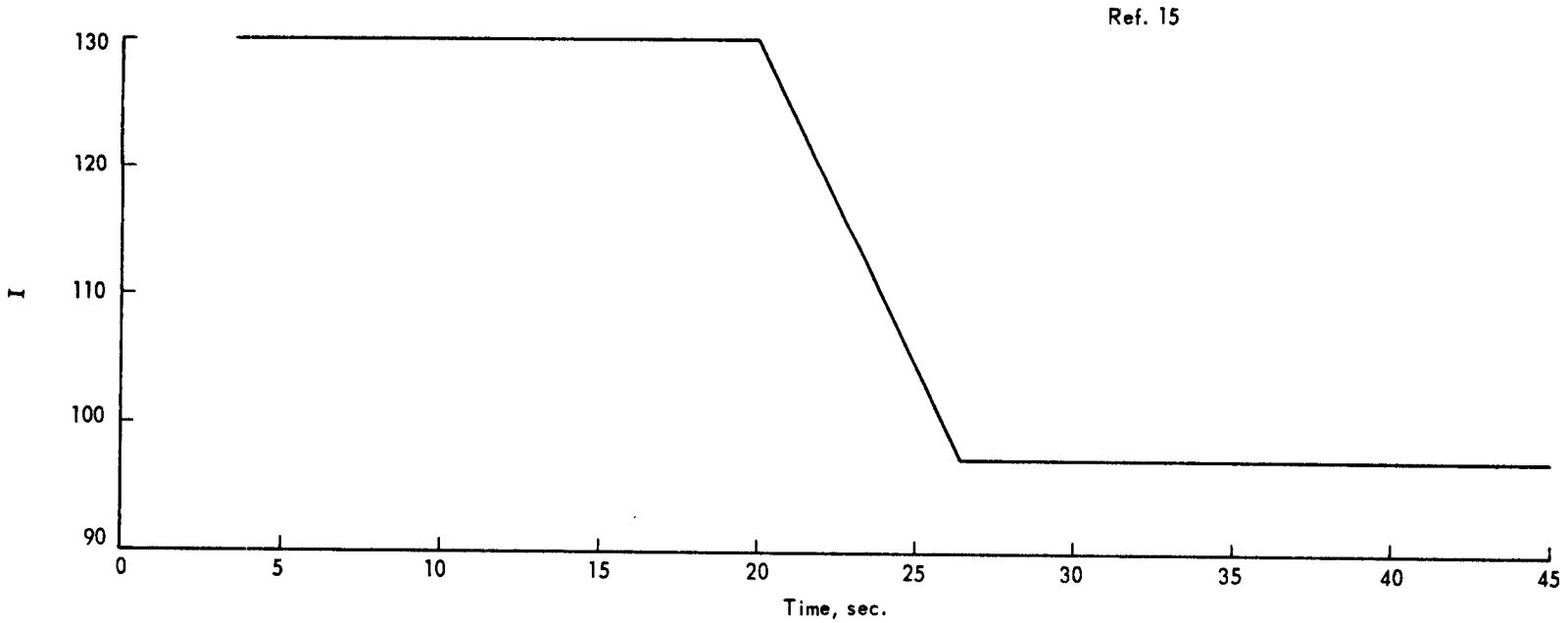

Figure A-13. Pitch Moment-of-Inertia History

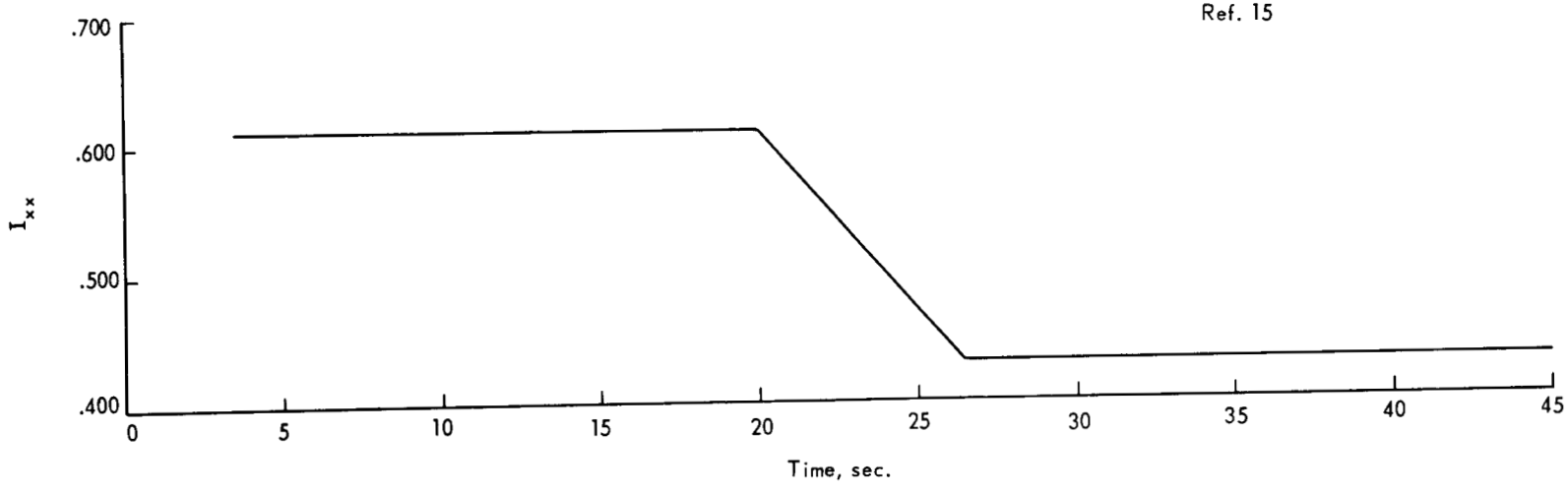

Figure A-14. Roll Moment-of-Inertia History